The Novel Role of Midbody-Associated mRNAs in Regulating Abscission

Trey Farmer[1], Ke-Jun Han[1], Katherine F. Vaeth[1,2], J. Matthew Taliaferro[2,3,4], and Rytis Prekeris[1,4]

1. Department of Cell and Developmental Biology, University of Colorado Anschutz Medical Campus, Aurora, CO, 80045
2. Department of Biochemistry and Molecular Genetics, University of Colorado Anschutz Medical Campus, Aurora, CO, 80045
3. RNA Bioscience Initiative, University of Colorado Anschutz Medical Campus, Aurora, CO, 80045
4. Corresponding authors: matthew.taliaferro@cuanschutz.edu; rytis.prekeris@cuanschutz.edu

Abstract
Midbodies (MBs) have been shown to function during telophase as a recruiting hub, especially for ESCRT-III complex subunits, including CHMP4B, to regulate the abscission step of cytokinesis. However, the molecular machinery governing specific protein targeting and activation at the MB remains poorly understood. Until recently, it was thought that abscission regulating proteins, such as ESCRT-III complex subunits, accumulate at the MB by directly or indirectly binding to the MB resident protein, CEP55. However, recent studies have shown that depletion of CEP55 does not fully block ESCRT-III targeting to the MB, and cells in CEP55 knock-out mice divide normally. Additionally, since MBs are microtubule-rich, proteinaceous structures, it is conceptually hard to imagine how large protein complexes, such as the ESCRT-III complex, can successfully diffuse into the MB from the cytosol in a rapid and highly regulated manner. Here, we show that MBs contain mRNAs and that these MB-associated mRNAs can be locally translated, thus, resulting in the accumulation of abscission-regulating proteins. We also demonstrate that localized MB-associated translation of CHMP4B is required for it's targeting to the abscission site. Finally, we demonstrate that 3'-UTR-dependent CHMP4B mRNA targeting to the MB is required for successful completion of cytokinesis. Based on all this data, we propose a novel method of regulating cytokinesis and abscission by MB-associated targeting and localized translation of selective mRNAs.

Introduction
The cell cycle is a key event during the development, growth, and reproduction of all organisms. Cytokinesis is the final stage of the cell cycle that results in the physical separation of two daughter cells. The mother cell divides by the formation of the cleavage furrow, leaving two daughter cells connected by a microtubule-rich intercellular bridge. Additionally, during ingression of the cleavage furrow, the central spindle microtubules are compacted to form a structure known as the midbody (MB). To complete cytokinesis, the intercellular bridge must be cleaved on one or both sides of the MB, via the process known as the abscission (Figure 1A). Abscission is a highly regulated event, and it is now well established that the MB plays a key role in regulating completion of cytokinesis by recruiting and activating abscission-mediating proteins, such as the Endosomal Sorting Complex Required for Transport (ESCRT-III) complex, as well as several regulators of the abscission checkpoint[1, 2]. While targeting and activation of abscission regulators at the MB is required for completion of cytokinesis, the mechanisms governing this process remain to be fully defined.

Previous studies have shown that several members of the ESCRT-III machinery are recruited to the MB just before initiation of the abscission[3-6]. Specifically, it was shown that TSG101 recruits

Charged Multivesicular Body Proteins (CHMPs, components of the ESCRT-III complex)[7] to the MB during telophase. In addition to TSG101, ALIX (also known as PDCD6IP) also contributes to the direct recruitment of the ESCRT-III complex to the MB[1, 4, 8]. Upon recruitment to the MB, the ESCRT-III components oligomerize (CHMP4B and CHMP2A or CHMP3 and CHMP6) into spiral structures with progressively smaller diameters towards the abscission site[9-11], the process that is thought to be responsible for the eventual abscission of the intercellular bridge to complete cytokinesis and form two daughter cells[6, 9, 10]. Inhibiting MB recruitment of ESCRT-III results in abscission defects, demonstrating the importance of appropriately regulating ESCRT-III protein accumulation and activation at the MB[5, 6, 12-15].

Until recently, it has been thought that TSG101 accumulates at the MB by binding to the MB resident protein, CEP55[3, 4, 6, 9, 10, 16, 17]. This binding was presumed to tether the TSG101 at the MB, gradually leading to ESCRT-III accumulation before initiation of abscission; however, recent studies have shown that depletion of CEP55 does not fully block ESCRT-III targeting to the MB, and CEP55 knock-out mice are able to grow and develop[18]. Finally, CEP55 is a protein present only in vertebrates, thus, while CEP55 clearly contributes to ESCRT-III recruitment to the MB, it does not appear to be absolutely required for abscission. Additionally, the MB and intercellular bridge are microtubule-rich, diffusion-limited structures, raising a question of how large protein complexes, such as the ESCRT-III complex, can rapidly diffuse via the intercellular bridge into the MB from the cytosol in a timely and efficient manner.

Recent work suggested that in addition to regulating abscission, secreted post-mitotic MBs (also known as MBsomes or Flemmingsomes) can be internalized by other cells where they regulate cell proliferation and differentiation[8, 19-24]. It was proposed that these MBsomes may mediate cell-to-cell transfer of various signaling molecules in a manner similar to exosomes and extracellular vesicles[23, 24]. Consequently, several laboratories, including ours, have analyzed the proteome of secreted MBsomes. Interestingly, these studies have shown that, in addition to various signaling proteins, MBs are also enriched in ribosomal and translation initiation factor proteins[8, 23-25], raising an intriguing possibility that MB-associated mRNA targeting and localized translation may mediate various mitotic and post-mitotic MB functions.

In this study we show, for the first time, that a specific subset of mRNAs is indeed targeted to and enriched at the MBs. We also demonstrate that MBs contain active ribosomes and that MB-associated protein translation is needed for successful completion of the abscission. Importantly, by using a combination of RNAseq, qPCR, and smFISH, we demonstrate that mRNA encoding ESCRT-III components, specifically CHMP4B, CHMP2A, CHMP3, and CHMP6, are all enriched at the MB, and that MB-associated translation is needed for CHMP4B accumulation at the MB during telophase. Finally, characterization of CHMP4B mRNA revealed that the 3'-UTR is critical for efficient CHMP4B mRNA targeting to the MB. Collectively, this study proposes a novel mechanism of regulating cytokinesis and abscission by MB-associated targeting and localized translation of selective mRNAs that include, but are not limited to, the members of ESCRT-III complex. These findings lay a foundation for future studies in determining the molecular mechanisms regulating mRNA targeting and translation at the MB, and future analyses of the roles that this mRNA targeting plays in regulating abscission and post-mitotic MBsome functions.

Results

Identification of Midbody-Associated mRNAs

Recent studies have shown that MBs are enriched in RNA-binding proteins[8, 23-25], leading to the intriguing idea that MBs may contain mRNAs, and that local translation at the MB may regulate various MB functions. To test this hypothesis, we first set out to determine whether specific

mRNAs actually accumulate at the MBs, and began by isolating MBsomes in triplicate from tissue culture media as previously described[26] (Figure 1A). We then prepared oligo-dT-based mRNA libraries from both MBsomes and matched whole cell RNA samples, analyzing them using RNAseq (Supplemental Table 1). To assess the reproducibility of the RNA content of our MBsome preparations and their relationship to whole cell RNA samples, we used principal components analysis and hierarchical clustering (Figure 1B, C). With both approaches, we found that the MB RNA samples were highly similar to each other, indicating the reproducible nature of their RNA contents. Importantly, they were well separated from the whole cell RNA samples, suggesting that the MB RNA samples contained an RNA composition distinct from that found in the whole cell samples. Overall, the RNAseq analysis identified 16,922 mRNAs that can be detected in the MBsome. From those, 378 mRNAs are significantly depleted, and 545 mRNAs are significantly enriched in the MBsomes as compared to the whole cell RNA samples (Figure 1D; Supplemental table 1).

To determine the possible function of these MB-enriched mRNAs, we performed a Gene Ontology (GO) Enrichment Analysis (Figure 2A) and found that mRNAs encoding for ribosomal proteins, as well as various translation regulators, are highly enriched in the MBsomes, consistent with the hypothesis that localized MB-associated translation may play an important function in MBs (Figure 2A). Furthermore, we found that mRNAs encoding for proteins that regulate cell cycle and microtubule dynamics are enriched at the MBsomes (Figure 2A). We also determined that mRNAs of several abscission-regulators, such as Citron Kinase, CDK11A, CDK11B, and AKTIP, are also enriched in the MBsomes (Figure 2B). Importantly, we found that mRNAs of the ESCRT-III complex proteins, CHMP4B, 2A, 3, and 6, were all enriched at the MBsome (Figure 2B-D). This is especially noteworthy as CHMP4B/2A and CHMP3/6 are known to co-polymerize and drive the final abscission step[9-11] (Figure 2D), suggesting that localized translation of ESCRT-III proteins may drive their accumulation at the MB and may also be required for the abscission step of cytokinesis.

Interestingly, not all of the mRNAs of genes associated with abscission were found to be enriched at the MBsomes. For example, CEP55, TSG101, ALIX, and VPS4 mRNAs, while present in MBsomes, were not enriched as compared to the whole cell transcriptome (Figure 2B-C). This suggests that only a subset of abscission regulating proteins, specifically proteins that act during final steps of the abscission, may be controlled by local translation. Consistent with this hypothesis, CEP55, TCG101, and ALIX regulate early steps of the abscission, namely recruiting and tethering ESCRT-III to the MB (Figure 2D). In contrast, all ESCRT-III components are recruited during late telophase, just before completion of the abscission, suggesting an intriguing possibility that the MB targeting of proteins during telophase may depend on localized translation of specific mRNAs after MB formation. In the rest of the study, we will test this hypothesis by focusing on the machinery mediating MB targeting and translation of CHMP4B mRNA.

Midbodies contain the molecular machinery required for protein translation

Our GO analysis (Figure 2A) demonstrated that numerous MB-associated mRNAs encode for proteins that regulate ribosomal assembly and function. This further supports the idea that MBs contain ribosomal machinery, which in turn can mediate local translation. Due to this finding, and the fact that CHMP4B mRNA is enriched in the MBs, we hypothesize that local translation of CHMP4B and other ESRCT-III subunits may contribute to ESCRT-III accumulation at the MB, therefore regulating the abscission. For this hypothesis to be correct, MBs must contain CHMP4B mRNA and translation associated ribosomal machinery, as well as being sites of active protein translation.

To test this idea, we first visualized CHMP4B mRNA using single molecule RNA *in situ* hybridization (smFISH)[27]. Consistent with our hypothesis that CHMP4B may be translated at the MB, we found that CHMP4B mRNA is present within the intracellular bridge during telophase (see arrows in Figure 3A). To validate the specificity of our CHMP4B smFISH probes, we depleted CHMP4B RNA using siRNA and observed a corresponding decrease in the number of observed CHMP4B RNA molecules per cell (Figure 3B).

There are multiple mechanisms that can drive mRNA accumulation at specific subcellular compartments. One is direct targeting of mRNA that is independent of translation, and another is co-translational targeting of mRNA that relies on the targeting of the nascent peptides (rather than mRNA) that emerge from the ribosome during translation. In this case, mRNA is indirectly accumulated to the specific subcellular compartment as the result of protein-dependent targeting of the entire mRNA-associated ribosome. To differentiate between these two possibilities, we briefly treated the cells with puromycin, a known inhibitor of protein translation that dissociates ribosomes from their mRNA substrates. As shown in Supplemental Figure 2A-C, puromycin treatment did not block CHMP4B mRNA accumulation at the MB, suggesting that localized protein translation is not required for the mRNA targeting to the MB.

Next, we set out to determine if ribosomal components that are needed for translation are also present at the MB. Initially, we analyzed three different proteomic datasets of purified MBsomes using The Database for Annotation, Visualization, and Integrated Discovery (DAVID)[8, 23, 24]. Consistent with the possibility of localized MB-associated translation, there are numerous ribosomal and translation initiation factor proteins present in the MB proteome (Figure 3C). Not only were there ribosomal and translation initiation factor proteins present in the proteomic datasets, but they were also highly enriched according to the DAVID analysis enrichment score (Figure 3C). Finally, upon staining HeLa cells with antibodies against Ribosomal Protein L3 (RPL3), we show the presence of RPL3 in the MB and intracellular bridge (marked by anti-Acetylated-Tubulin antibodies) (Figure 3D-F). While this does not prove that local translation is occurring, it supports the idea that the ribosomal translation machinery is present at the MB and can potentially perform active translation of MB-associated mRNAs.

Midbodies are sites for active translation

While the presence of ribosomal machinery at the MB supports the idea of local MB-associated protein translation, it is yet to be shown that active translation occurs at the MB and intracellular bridge during late telophase. To test this possibility, we used puromycin as a marker for active translation. Puromycin inhibits translation by causing the formation of a puromycylated nascent peptide chain and leading to dissociation of ribosomes and premature chain release. Importantly, these puromycylated peptides accumulate at sites of active translation and can be detected using anti-puromycin antibodies. To test whether translation occurs at the MB, we treated HeLa cells for 10 min with either DMSO or puromycin. We found that an anti-puromycin signal in MBs can be observed in puromycin-treated cells (Figure 4A-D), and, importantly, pre-treatment of cells with cycloheximide (Figure 4A) blocked the anti-puromycin signal (Figure 4A-D). Cycloheximide functions by interfering with the translocation step in protein synthesis, thus preventing ribosomes from incorporating puromycin in nascent peptides. Finally, anti-CHMP4B and anti-puromycin signals co-localized at the MB and intercellular bridge (Figure 4E-H). All together, this data demonstrates the presence of active translation at the MB at the same time that CHMP4B is accumulating during telophase.

Active translation is required for the accumulation of CHMP4B at the MB during late telophase

Since we have been able to show that local translation does occur in the MB, and that the anti-puromycin signal co-localizes with CHMP4B, we hypothesized that inhibiting protein translation at the MB should affect CHMP4B accumulation at the MB during late telophase. To test this hypothesis, we briefly (1 hour) treated HeLa cells with puromycin to block translation and analyzed CHMP4B levels at the MB by immunofluorescence microscopy. Consistent with our hypothesis, puromycin-treatment decreased CHMP4B intensity in the MB (Figure 5A-C). CHMP4B levels were also slightly reduced in the cell body, although to a much lesser (and statistically not significant) extent than seen in the MB (Figure 5A, D, and E).

Puromycin blocks all protein translation. Consequently, even a short puromycin treatment will impact many proteins, thus, it is possible that inhibition of translation also affects other MB proteins. To further bolster this idea, we chose to look at CEP55, a protein that is recruited to the MB during its formation and is required for MB-accumulation of TSG101 and ESCRT-III complex (including CHMP4B) [3, 4, 6, 9, 10, 16, 17]. Since CEP55 mRNA was not found to be enriched in our RNAseq analysis (Figure 2B), it presumably does not require MB-associated translation for its targeting. Consistent with this hypothesis, puromycin treatment did not have any effect on CEP55 intensity in the MB or cell body (Figure 5F-J).

If localized translation of CHMP4B, and presumably other members of the ESCRT-III complex, is required for their accumulation at the MB, we would expect that inhibition of translation during telophase would affect the cells' ability to undergo abscission, thus, arresting them at late telophase. To test this hypothesis, we counted the number of cells in telophase and found that 1 hour of treatment with puromycin significantly increased the number of cells in telophase (Figure 5K), while decreasing the number of cells that have just undergone abscission (Figure 5L; Supplemental Figure 3A-D), which are all indications of defects in cell division.

While the previous experiments support the idea that local translation of CHMP4B is at least partially responsible for the accumulation of CHMP4B during telophase, it does not exclude other mechanisms for CHMP4B accumulation at the MB. Since it has been proposed that CEP55 is the key initial recruiter of abscission-related proteins in mammalian cells, it is plausible that both pathways are required for efficient recruitment of ESCRT-III during abscission. To further test this idea, we used a combination of puromycin, CEP55 siRNA, or CEP55 siRNA/puromycin treatments to test their effect on CHMP4B accumulation in the MB. As we already have shown, puromycin treatment alone caused a significant reduction in CHMP4B intensity at the MB (Figure 5M-O). Similarly, consistent with previous reports, CEP55 knock-down (Supplemental Figure 1B) also decreased CHMP4B intensity at the MB (Figure 5M-O). Surprisingly, a combination of CEP55 KD and puromycin treatment did not further reduce CHMP4B intensity at the MB, suggesting that local MB-associated translation and CEP55 may work together to allow efficient accumulation (by localized translation) and retention (by tethering CHMP4B at the MB) of CHMP4B during late telophase.

Short puromycin wash-out recovers CHMP4B levels at the MB but not cell body

While our previous data shows that protein translation contributes to CHMP4B accumulation at the MB, the data is difficult to interpret because puromycin also resulted in a slight decrease of CHMP4B levels at the cell body. Thus, we cannot differentiate between two possibilities: (1) CHMP4B targeting relies on MB-associated translation during telophase; (2) CHMP4B is translated at the cell body and then simply diffuses back to the MB. To help differentiate between those two possibilities we performed a puromycin wash-out experiment (Figure 6). Briefly, we treated cells with puromycin for 1 hour, followed by a quick puromycin wash-out and incubation of cells for 5 or 10 minutes, before analyzing the levels of CHMP4B in the MB and the cell body. As we already have shown, puromycin treatment resulted in decreased CHMP4B

levels in both the MB and the cell body (Figure 6A-E). Importantly, after puromycin wash-out, CHMP4B levels at the MB started to increase within 5 min, with a complete recovery after 10min (Figure 6A, B-C). On the contrary, CHMP4B intensity in the cell body did not recover even after 10min (Figure 6A, D-E), suggesting that CHMP4B accumulation at the MB is primarily driven by localized translation rather than by diffusion of CHMP4B from the cell body.

Since CHMP4B levels rapidly recover at the MB after the puromycin wash-out, this should also lead to a rapid recovery of the cell's ability to undergo abscission. Consistent with this idea, 5 minutes after the puromycin wash-out, cells fully recovered their ability to undergo abscission, as determined by a decrease in number of cells in telophase and increase in number of cells that have just undergone abscission (Figure 6F). All this data suggests that CHMP4B accumulation at the MB depends on local translation rather than diffusion from the cell body, and that MB-associated translation of CHMP4B is required for successful completion of the abscission.

The 3'-UTR enhances CHMP4B protein accumulation at the MB

Up to this point, we have been able to show that CHMP4B mRNA is present in the MB, local translation can occur at the MB, and that CHMP4B accumulation at the MB is, at least partially, regulated by local translation. The next logical step is to determine how the CHMP4B mRNA is targeted to the MB. RNA trafficking is often driven by cis-regulatory elements that are commonly found in the 5'- or 3'-UTRs[28]. To that end, we generated clones containing the 5'- and/or 3'-UTR of CHMP4B fused to RFP-CHMP4B cDNA. One major issue with transient expression is the high variation in expression levels in different cells hindering our ability to tell whether differences in MB targeting of various CHMP4B constructs are due to UTRs or due to the differences in expression levels. To minimize this issue, we used a HeLa LoxP recombination system[29]. Briefly, this system allows for high-efficiency and low-background recombination-mediated cassette exchange technology[29]. This system allowed us to obtain a virtually homogenous cell pool containing various doxycycline inducible CHMP4B constructs, and importantly, each cell will have one copy of the construct that is inserted in the same genomic locus. Upon making cell lines containing various CHMP4B constructs, we first used immunofluorescence microscopy, western blotting, and qPCR to confirm that doxycycline does induce the expression of these constructs (Supplemental Figure 4A-G). Interestingly, we found that the presence of 3'-UTR without the 5'-UTR slightly deceased CHMP4B mRNA levels, raising the possibility that the 3'-UTR of CHMP4B may also regulate mRNA stability (Supplemental Figure 4B and E). Additionally, please note that the insertion of the 5'-UTR generated an alternative start codon that was in frame with the RFP, resulting in two CHMP4B bands (Supplemental Figure 4F).

To determine the role of UTRs in CHMP4B targeting, we first tested whether having the 5'- and/or 3'-UTR resulted in more efficient RFP-CHMP4B accumulation in the MB. To that end, we calculated the ratio of RFP-CHMP4B protein intensity at the MB and cell body. As shown in the figure 7A-C, the presence of the 3'-UTR significantly enhanced RFP-CHMP4B enrichment at the MB as compared to RFP-CHMP4B alone (Figure 7A-C). Interestingly, the 5'-UTR alone did not enhance RFP-CHMP4B targeting to the MB, nor did it enhance the effect of 3'-UTR (Figure 7A-C). All this data suggests that the 3'-UTR plays an important role in mediating CHMP4B protein accumulation in the MB during telophase, presumably due to targeting and localized translation of RFP-CHMP4B mRNA. Consistent with previous reports, RFP-CHMP4B without UTRs is still able to accumulate in the MB, potentially showing that there are multiple mechanisms, such as CEP55 binding, that drives ESCRT-III targeting during abscission.

It has been previously reported that over-expression of exogenous tagged ESCRT-III members inhibits abscission[13]. Consistent with those studies, we also see an increase in multinucleation and the number of telophase-arrested cells in the cells overexpressing RFP-CHMP4B (Figure 7D-E). While the cause of this inhibition remains to be fully understood, it has been suggested that CHMP4B overexpression may lead to accumulation of cytosolic ESCRT-III aggregates, thus, sequestering the rest of the ESCRT-III subunits away from the MB. We wondered whether the inhibitory effect of exogenous CHMP4B may be due to the fact that it's mRNA lacks localization elements mediating targeting of CHMP4B to the MB. Consistent with this hypothesis, the effect of over-expression on multinucleation or telophase arrest was reversed in cell lines expressing RFP-CHMP4B constructs containing 3'-UTR (Figure 7D-E).

3'-UTR is required for targeting CHMP4B mRNA to the MB

Since the 3'-UTR is important for CHMP4B protein accumulation at the MB during abscission, one would expect that the 3'-UTR is also important for CHMP4B mRNA targeting to the MB. To determine that, we first analyzed RFP-CHMP4B mRNA localization using smFISH probes against CHMP4B. Consistent with the requirement of the 3'-UTR for RFP-CHMP4B accumulation, we observed smFISH signal in the MB of cells only expressing the RFP-CHMP4B-3'UTR construct (Figure 7F). One drawback of using smFISH in the MB is that it is only semi-quantifiable due to not knowing how efficiently the probes are able to penetrate the protein-rich region. To better quantify the difference between RFP-CHMP4B mRNA targeting to the MB, we purified MBsomes from cell lines expressing various constructs and analyzed mRNA levels by performing RT-qPCR on purified MBsomes and then compared them to whole cell mRNA levels. To measure only exogenous CHMP4B, we used primers designed to target the RFP sequence. As shown in Figure 7G, the presence of the 3'-UTR is required for efficient RFP-CHMP4B mRNA targeting to the MB, as compared to the amount of RFP alone or RFP-CHMP4B mRNA without 3'-UTRs (Figure 7G). This data suggests that the 3'-UTR is required for efficient RFP-CHMP4B mRNA targeting to the MB. Interestingly, RFP-CHMP4B without UTRs was also slightly enriched at the MB as compared to RFP alone. This slight mRNA enrichment could be due to co-translational RFP-CHMP4B mRNA accumulation at the MB. To test this possibility, we removed the start codon and generated a HeLa cell line expressing doxycycline-inducible RFP-CHMP4B-NoStart construct (Supplemental Figure 4C and E) and tested whether this mRNA also accumulates at the MBs. As shown in Figure 7E, removal of the start codon did not affect the ability of RFP-CHMP4B mRNA to accumulate at the MB, although it was clearly still much lower than RFP-CHMP4B-3'UTR. All this data suggests that the 3'-UTR is required for efficient CHMP4B mRNA targeting, although the coding sequence also appears to contribute to mRNA accumulation at the MB.

To test whether the 3'-UTR of CHMP4B is sufficient for the targeting of any mRNA to the MB, we generated a doxycycline inducible RFP-only, containing the 3'-UTR from CHMP4B (RFP-3'UTR; Supplemental Figure 4D and E) and tested the mRNA levels at the MB. While the 3'-UTR of CHMP4B did slightly enhance the levels of RFP mRNA at the MB, it did not reach the levels of RFP-CHMP4B-3'UTR mRNA (Figure 7E). This suggests that while CHMP4B 3'-UTR is essential for mRNA targeting, it may require other targeting elements that are possibly present in the CHMP4B coding region or secondary structure of the coding region to get the full translocation to the MB. This would also explain the slight, although not significantly different, increase in RFP-CHMP4B mRNA (without UTRs) at the MB as compared to RFP alone.

Discussion

The midbody (MB) is a microtubule-rich structure that forms at the end of cytokinesis as the result of compacting central spindle microtubules during cleavage furrow ingression. Even though the MB was first identified over a hundred years ago, only in the last decade has it

become apparent that the MB is not simply a byproduct of cell division, but plays many important roles. It is now well-established that the MB plays the role of a scaffolding platform that recruits and activates many abscission regulating proteins, such as Aurora B kinase, MKLP1, and ESCRT-III complex[16, 30-33]. Furthermore, recent studies have also shown that during cell division MBs can be released in the extracellular milieu where they are called MBsomes of Flemmingsomes[8, 23]. Uptake of these MBsomes by other cells can lead to changes in cell fate, differentiation, and proliferation capacity, presumably by mediating lateral transfer of specific signaling molecules[23, 24, 34]. However, what remains unclear is what these signaling molecules are and how they may affect cells after MBsome internalization. In this study we demonstrate that MBsomes contain a specific subset of mRNAs, many of them encoding proteins regulating cell division and differentiation. That raises a very intriguing possibility that delivery of specific mRNAs to the acceptor cells is what mediates post-mitotic MBsome functions, although further research will be needed to fully define the role of MBsome-dependent mRNA delivery.

Our study shows that MBs contain mRNAs encoding for several ESCRT-III components, namely CHMP2A, CHMP3, CHMP4B, and CHMP6. What makes this discovery especially exciting is that all these ESCRT-III complex proteins are known to co-oligomerize and drive the abscission step of cytokinesis. While the role of the ESCRT-III proteins in mediating abscission was first described over a decade ago[6, 9, 15], how ESCRT-III subunits are delivered and targeted to the MB remains somewhat controversial. Until recently, it has been thought that TSG101 and the ESCRT-III complex accumulate at the MB by directly or indirectly binding to MB resident protein, CEP55[3, 4, 6, 9, 10, 16, 17]. However, recent studies have shown that depletion of CEP55 does not fully block ESCRT-III targeting to the MB, and CEP55 knock-out mice are able to grow and develop with limited defects[18]. Additionally, CEP55 is only present in vertebrates, raising a question of how the ESCRT-III may be targeted in other organisms. Finally, the MB and intercellular bridge are packed with dense and heavily crosslinked microtubule bundles[35, 36], thus, creating a diffusion-limited environment. This raises the question about how large protein complexes, such as the ESCRT-III complexes, can rapidly diffuse via the intercellular bridge into the MB from the cytosol in a timely, efficient, and highly regulated manner. The discovery that ESCRT-III mRNAs are enriched at the MB suggests an intriguing possibility that regulated localized translation of ESCRT-III components contribute to accumulation of ESCRT-III at the MB during abscission.

Consistent with the hypothesis that localized protein translation contributes to ESCRT-III targeting to the MB, we show that the MB has all the components needed for translation. We also use anti-puromycin antibodies to demonstrate that active translation is occurring in the MB. Finally, we show that inhibition of protein translation during late telophase blocks completion of cytokinesis. Based on all these findings, we chose to further investigate one of the most important regulators of late-stage abscission, CHMP4B. There are several pieces of evidence suggesting that CHMP4B is being actively translated in the MB during telophase. First, CHMP4B co-localizes with anti-puromycin signals at the MB. Second, inhibition of protein translation during telophase leads to decrease in CHMP4B accumulation at the MB. Third, wash-out of puromycin (protein translation inhibitor) results in a very fast recovery of CHMP4B levels at the MB, which could not be explained by simple diffusion of CHMP4B from the cell body. Importantly, the ability of the cell to complete abscission also recovers within a similar timescale. All of this data suggests that CHMP4B can be locally translated and that it is at least partially responsible for the accumulation and function of CHMP4B at the MB.

Local translation of CHMP4B at the MB depends on the targeting of CHMP4B mRNA to the MB during telophase. What remains unclear is the molecular machinery governing mRNA delivery

and accumulation at the MB. It has been previously shown that the subcellular targeting of mRNAs is usually driven by cos-localization elements that are commonly found in the 5'- or 3'-UTRs[28]. Consequently, we tested whether the 5'- and 3'-UTRs are driving the translocation of CHMP4B mRNA to the MB. Our data demonstrates that the 3'-UTR is required for translocation and accumulation of CHMP4B at the MB. To test whether the 3'-UTR is sufficient for mRNA accumulation at the MB, we added CHMP4B 3'UTR to RFP and analyzed its ability to drive RFP mRNA accumulation at the MB. Interestingly, while we did see an increase in the levels of MB-associated RFP mRNA, the amount of RFP-3'UTR mRNA did not fully recapitulate the levels of RFP-CHMP4B-3'UTR, suggesting that the CHMP4B coding region may also play a role in CHMP4B mRNA targeting to the MB. While identification of specific MB-targeting elements remains to be completed, initial analysis identified several GA-rich motifs within the CHMP4B 3'-UTR. It has been previously shown that GA-rich motifs mediate targeting of Rab13 mRNA targeting to the actin rich cellular protrusions[37, 38]. Similarly, GA-rich motifs in Net1 mRNA were shown to mediate Net1 targeting to neurites[39]. Our RNAseq analysis of purified MBs showed Rab13 and Net1 mRNAs are also enriched in the MB, suggesting that the GA-rich motifs may also mediate CHMP4B mRNA targeting to the MBs. Interestingly, a recent study has shown that microtubule plus-end motor, Kinesin-I, may be responsible for transport of mRNAs in neurons and polarized epithelial cells[40]. This type of transport would be perfect for targeting mRNAs to the MB, because plus-ends of microtubules are oriented toward the MB, and Kinesin-I has already been implicated in transporting endosomes to the MB during cell division[41]. All these findings hint at a common mechanism that regulates subcellular targeting of mRNAs, although further evidence will be needed to fully determine that.

Taken together, this is the first study to demonstrate that a specific subset of mRNAs are targeted and enriched at the MB during cell division, and play a role in MB function during abscission (Figure 8). At least some of these mRNAs, such as CHMP4B mRNA, appear to be translated at the MB, and this translation plays a key role in accumulation of ESCRT-III components at the MB, thus regulating the abscission step of cytokinesis (Figure 8). While working out the details governing mRNA targeting and translation at the MB will require future studies, this work lays a foundation for identification of a novel mechanism regulating abscission. Finally, this study will not only advance our understanding of the machinery governing ESCRT-III translocation and accumulation at the MB, but it could also provide novel insight into the mechanisms of RNA targeting to other subcellular compartments and other cell types, as well as providing a framework for studying the role of mRNAs in the post-mitotic MB function (Figure 8).

Materials and Methods

Cell culture

All HeLa cell lines were kept in a 37 °C humidified incubator at 5% CO2, routinely tested for mycoplasma, and were maintained in DMEM with 10% FBS and 1% penicillin/streptomycin.

Reagents and antibodies

iTaq Universal SYBR Green Supermix was purchased from Bio-Rad. TRIzol, Puromycin, Doxycycline, Lipofectamine 2000, and Lipofectamine RNAiMax was purchased from Thermo Fisher Scientific. Stellaris Hybridization, Wash A, and Wash B Buffers were purchased from Biosearch Technologies. Hoechst stain was purchased from AnaSpec. Antibodies against the following proteins were used: RPL3 (Bethyl Laboratories #A305-007A,1:100 for immunofluorescence), Acetylated-Tubulin (Cell Signaling #D20G3, 1:500 for immunofluorescence), Acetylated-Tubulin (Millipore Sigma #T7451, 1:500 for immunofluorescence), CHMP4B (Proteintech #16639-I-AP, 1:300 for immunofluorescence), CEP55 (Abnova #H00055165-A01, 1:500 for immunofluorescence), RFP (Chromotek #6g6-20,

1:2000 for immunoblotting), Beta-Actin (LI-COR #926-42210, 1:2000 for immunoblotting), donkey anti-mouse-IgG conjugated to Alexa Fluor 488 (Jackson #715-545-150, 1:100 dilution for immunofluorescence), donkey anti-mouse-IgG conjugated to Alexa Fluor 594 (Jackson #715-585-1500, 1:100 dilution for immunofluorescence), donkey anti-rabbit-IgG Alexa Fluor 488 (Jackson #711-585-152, 1:100 dilution for immunofluorescence), and donkey anti-rabbit-IgG conjugated to Alexa Fluor 594 (Jackson #711-585-152, 1:100 dilution for immunofluorescence), donkey anti-mouse IRDye 680CW (LI-COR #926-32212, 1:5000 for immunoblotting), and donkey anti-rabbit IRDye 800CW (LI-COR #926-68072, 1:5000 for immunoblotting).

RNA isolation and quantitative PCR

RNA was extracted using Trizol (Thermo Fisher #15596026) per the manufacturer's instructions. The RNA was reverse transcribed using SuperScript IV (Thermo Fisher, #18091050) per the manufacturer's instructions. Quantitative PCR was performed using iTaq Universal SYBR Green Supermix (Bio-Rad, #1725121). Primer sequences can be found in Table 1. To quantify the RT-qPCR, each cDNA sample was normalized to GAPDH. If the experiment was looking at enrichment in MBsomes, the data is represented as a ratio of the normalized MB/normalized total cell.

Table 1. RT-qPCR primer sequences

RT-qPCR Primer Name	Primer Sequence 5' to 3'
CHMP4B Forward	GCTGCGGGACACGGAAGAGA
CHMP4B Reverse	TTCATGGCCTTGGCGGCATAGC
RFP Forward	GGCCACGAGTTCGAGATCGAG
RFP Reverse	TAGTCGGGGATGTCGGCGGG
CHMP2A Forward	GAACCGTGCCATGCGGGAGC
CHMP2A Reverse	GTGCGCACCAAGTCTTTTGCC
CHMP6 Forward	GAAGCAGCAGCGGGACAAGCT
CHMP6 Reverse	GCTTCTTCTTGAGCAGCAGCT
CHMP3 Forward	CGATCTGTGAAAGATGCTGCC
CHMP3 Reverse	ACAACTCCCTCATGGTGGCCT
CEP55 Forward	GAGAAGAATGCTTATCAACTC
CEP55 Reverse	TCTTCAGATAAGGCTTTCAAC
TSG101 Forward	CCAATATGCCTATGGCTACTG
TSG101 Reverse	AAGTCTGACTGTGGGTGTTTC
GAPDH Forward	CTGGGCTACACTGAGCACC
GAPDH Reverse	AAGTGGTCGTTGAGGGCAATG

MB purification and RNAseq

Midbodies were isolated as previously described[26]. Briefly, media from the various HeLa cells was collected and subjected to a series of centrifugation spins (300 × g, 10,000 × g). Sucrose gradient fractionation was performed at 3000×g, and the interphase between 40% glycerol and 2□M sucrose was collected, spun at 10,000 × g to pellet the midbodies. RNA was extracted using TRIzol (Thermo Fisher #15596026) per the manufacturer's instructions. For control and MB group 1, the library prep and RNAseq was performed by the University of Colorado

Anschutz Medical Campus Genomics facility. The Genomics facility generated a poly A enriched library from the total RNA extraction and performed RNAseq on an Illumina HiSeq2000 platform, utilizing 1 lane, single read 125 cycles. For control group and MB group 2 and 3, the library prep and RNAseq was performed by Novogene. Briefly, Novogene generated a poly A enriched library from the total RNA extraction and performed RNAseq on a NovaSeq PE150 platform with 6 G raw data per sample.

RNAseq data processing

Transcript abundances were calculated using Salmon v1.9.0[42] using the flags –seqBias and –gcBias. Transcript abundances were collapsed to gene level using txImport [cite: https://f1000research.com/articles/4-1521/v1]. To determine enrichment of genes in the midbody, DEseq2 [cite: https://genomebiology.biomedcentral.com/articles/10.1186/s13059-014-0550-8] was used to calculate the log2 ratio of midbody/whole cell counts and identify significantly enriched RNAs. Genes with a basemean (average of normalized count values) less than 250 were excluded. Plots were generated in Rstudio using R version 4.1.1.

siRNA transfections

Custom CHMP4B siRNA oligonucleotides (Dharmacon, AUCGAUAAAGUUGAUGAGUUAUU) and custom CEP55 siRNA oligonucleotides (Millipore Sigma, AGGCAUGUACUUUAGACUU) were transfected into HeLa cells using Liptofectamine RNAiMAX with 40nM oligonucleotide. The efficiency of the knock-down was measured 72 h post transfection by RT-qPCR (previously described above).

Immunofluorescence and quantification

HeLa cells were treated as indicated in the text and then fixed in 1% paraformaldehyde in PBS for 10 min at room temperature. Cells were rinsed three times in PBS. The cells were then incubated with primary antibody in PBS containing 0.5% BSA and 0.2% saponin for 1 h at room temperature, washed three times in PBS and then incubated with the appropriate fluorochrome-conjugated secondary antibodies diluted in PBS containing 0.5% BSA and 0.2% saponin for 30 min. Cells were washed three times in PBS and mounted in Fluoromount (Southern Biotech).

Fixed cells were imaged with an inverted Axiovert 200M microscope (Zeiss) with a × 63 oil immersion lens and QE charge-coupled device camera (Sensicam). Z-stack images were taken at a step size of 500–1000 nm. Image processing and quantification was performed using 3i Slidebook 6 software (Intelligent Imaging Innovations). Briefly, masks were made to calculate the total intensity of the cell body or the intercellular bridge as well as the total area for each mask. The numbers were then used to calculate the intensity/micron^2. Unless otherwise stated, all images are represented as a maximal projection of the z-stack.

smFISH probe design

The smFISH protocol was adopted from Tsanov *et al*[27]. Briefly, probes were designed by inputting the CHMP4B sequence into the Oligostan software. CHMP4B probes then had a Y flap (TTACACTCGGACCTCGTCGACATGCATT) added in order to have a location where we can hybridize the fluorescent molecules to the probe. The sequences can be found below. The fluorescent probe was designed by taking the reverse compliment of the Y flap (AATGCATGTCGACGAGGTCCGAGTGTAA) and adding Alexa488 or Alexa594 to both ends.

Probe #	Probe Sequence from 5' to 3'
1	CAGGTCATTTCAACTGCAACCAGTCGACCTTACACTCGGACCTCGTCGACATGCATT
2	TTCCATTGAGGATTCAGCAGTGGAGTCAGCTTACACTCGGACCTCGTCGACATGCATT
3	CCCAGGTGCAGACCATGCTATGCAGATTACACTCGGACCTCGTCGACATGCATT
4	CTTCTCCAAACCCTACAGGTTTCGAAATTGCTTACACTCGGACCTCGTCGACATGCATT
5	AGCCTATGGCTTTTGAAAAATGACTTTTCTGCTTACACTCGGACCTCGTCGACATGCATT
6	CAGCGCTGGACCCCATTACATGGATCTTACACTCGGACCTCGTCGACATGCATT
7	GCCCAGTTCTCCAATTCCTTCATGTCTTACACTCGGACCTCGTCGACATGCATT
8	CTGTTTCGGGTCCACTGATTTCCAGCAAATTTACACTCGGACCTCGTCGACATGCATT
9	TTGTCTAGTTCCTCCTGTTCTAGTTCTTCTATTACACTCGGACCTCGTCGACATGCATT
10	TCCGCCATGAGCTCATCCTCGTCAAATTACACTCGGACCTCGTCGACATGCATT
11	TTGAAATCTCCTCTGCAAGTTCTTGCTGGTTACACTCGGACCTCGTCGACATGCATT
12	ATGTCCATGTTGTCATGGGCCGCCTTTTACACTCGGACCTCGTCGACATGCATT
13	CCTTGGCGGCATAGCCCATGTTCTTGTTACACTCGGACCTCGTCGACATGCATT
14	CCAGCTGCTTCTCATACCTCTTCTTATTACACTCGGACCTCGTCGACATGCATT
15	CCTGGAGGGCCGCGCGCTTGTTTTTGTTACACTCGGACCTCGTCGACATGCATT
16	GCCGTCAGCTCCTGCTCGATTTTCTTTTACACTCGGACCTCGTCGACATGCATT
17	CCAGGAACTCCTGTTTCTTGCTTAACATCTTTACACTCGGACCTCGTCGACATGCATT
18	ATGTATGCACGTTTCCAATGAGTTATCTATCATTACACTCGGACCTCGTCGACATGCATT
19	TATCACAAACAGCAACAAGGACCTTATAGCTATTACACTCGGACCTCGTCGACATGCATT
20	TGGAACTTAATTCTAACAATCTCACTTGCTCTTTACACTCGGACCTCGTCGACATGCATT
21	AGAGAACACCATCCATTTCAAATCAATGTCACTTACACTCGGACCTCGTCGACATGCATT
22	ACTCCAGAAGACCAGGGGAGCAAGGGGTTACACTCGGACCTCGTCGACATGCATT
23	GAGGAGTGGGCCAGAGTGGTAAACACAGGGTTACACTCGGACCTCGTCGACATGCATT
24	AATACACAGGTGATGGACAGAAACACAGCTCTTACACTCGGACCTCGTCGACATGCATT
25	GTACCGTACAAGTACACAAAGAGATGTGCGGCTTACACTCGGACCTCGTCGACATGCATT
26	GTCAACTGACTTACAAGGACAGAGGCTACATTTACACTCGGACCTCGTCGACATGCATT
27	GTCCAGAAGCTCAATGTTGGATTTGCAAATACTTACACTCGGACCTCGTCGACATGCATT
28	AAATTCAACATTATAAACAGCAGGCACTTCCCTTACACTCGGACCTCGTCGACATGCATT
29	CAACGCGGCCCTACTGCTTTGGAGTGTTACACTCGGACCTCGTCGACATGCATT
30	AGTCGAAAGCGATGGAACCTGCCTGCATTACACTCGGACCTCGTCGACATGCATT
31	CGTCCTCCTCTTCTTTCTTCTTGGCGTTACACTCGGACCTCGTCGACATGCATT
32	GGTAGGGCTATAGAGGGAACATTTGGTAGAGGTTACACTCGGACCTCGTCGACATGCAT T
33	AGCAATGTCCTGCATTAACTCATCAACTTTATTACACTCGGACCTCGTCGACATGCATT
34	CACCTCGGTGTTGGTGTTGGCATTCTCTTACACTCGGACCTCGTCGACATGCATT
35	CCTCCCGCTGGAACTCGATGGTTGATTTACACTCGGACCTCGTCGACATGCATT
36	CCGAACAGCTTCCCGAACACCGACATTTACACTCGGACCTCGTCGACATGCATT
37	TCAAAATCAGATGCATTATTACAGCTAAGGGCTTACACTCGGACCTCGTCGACATGCATT

smFISH visualization
HeLa cells were plated on collagen coated coverslips and allowed to grow to 70-75% confluency. The media was aspirated, and cells were washed once with 1x PBS. Cells were fixed in 1% PFA for 10 min at room temperature, then washed twice with 1x PBS. Cells were permeabilized with 0.1% TX-100 for 5 min at room temperature. The cells were washed with Wash Buffer A (Stellaris) at room temperature for 5 min. In the meantime, the CHMP4B probes and Y flap was hybridized using the protocol from Tsanov *et al*[27]. 2µl of the probe/flap hybridization product was added to 100µl of hybridization buffer (Stellaris). A hybridization chamber was prepared using an empty 15cm cell culture plate, wrapped in tinfoil with wet paper towels surrounding the rim on the inside, and parafilm covering the bottom of the plate. 100µl of the hybridization solution was added to the parafilm and the collagen coated coverslip were placed with cell side down, facing the hybridization solution. The hybridization chamber with the coverslips was incubated at 37°C overnight. Next day, the glass coverslips were transferred to a fresh 6-well plate with the cell side up and incubated with Wash Buffer A (Stellaris) and Hoechst stain (1:2000, AnaSpec) at room temperature in the dark for 30 min. Hoechst stain was washed with Wash Buffer B at room temperature in the dark for 5 min. Coverslips were then mounted upside-down onto slides with Fluoromount G (Southern Biotech) and sealed with clear nail polish. Slides were imaged using an inverted Axiovert 200M microscope (Zeiss) with a × 63 oil immersion lens and QE charge-coupled device camera (Sensicam).

smFISH particle counting
ImageJ was used to count the total number of smFISH particles. First, the channels were separated, and an outline of the cell was drawn using the freehand tool in the smFISH channel. Next, a threshold was set using a control cell. The threshold set with the control cell was used for all cells after that. Finally, the particles were analyzed to get the total number of particles in each cell.

Puromycin treatment
HeLa cells were plated on collagen-coated coverslips and allowed to grow to 70-75% confluency. At this time, cells were exposed to 25µM puromycin and incubated at 37°C for 1 h. Cells were then fixed, stained, and imaged as previously described.

Anti-Puromycin labeling
HeLa cells were plated on collagen-coated coverslips and allowed to grow to 70-75% confluency. At this time, the cells were either treated with DMSO (volume equal to that of the other treatments) for 40 min at 37°C, 50µM cycloheximide for 40 min plus the last 10 min with 25µM puromycin at 37°C, or only 25µM puromycin for 10min at 37°C. Cells were then fixed, stained, and imaged as previously described.

Puromycin Wash-Out Assay
HeLa cells were plated on collagen-coated coverslips and allowed to grow to 70-75% confluency. At this time, the cells were either untreated, treated with 25µM puromycin at 37°C for 1 h, treated with 25µM puromycin at 37°C for 1 h, washed with 1x PBS and allowed to recover for 5 min in complete media at 37°C, or treated with 25µM puromycin at 37°C for 1 h, washed with 1x PBS and allowed to recover for 10 min in complete media at 37°C. Cells were then fixed, stained, and imaged as previously described.

Generation of doxycycline-inducible constructs

Due to the GC rich nature, we were unable to PCR the full-length 3'-UTR. Therefore, we used Twist Bioscience to generate a modified sequence that we could use for a template (TGGGGTCCAGCGCTGGCTGGGCCCAGACAGACTGTGGTGGCCTGCGCAGCGAGCAGGC GTGTGCGTGTGTGGGGCAGGCAGGATGTGGTGCAGGCAGGTTCCATCGCTTTCGACTCTC ACTCCAAAGCAGTAGGGCCGCGTTGCTGCTCACTCTCTGCATAGCATGGTCTGGAAGTGT GCTGTTTATAATGTTGAATTTCTGTAAAATAAACTGTATTTGCAAATCCAACATTGAGCTTCT GGACTACGCTGACTCCACTGCTGAATCCTCAATGGAAAGGGTCGACTGGTTGCAGTTGAA ATGACCTGAAATGTAGCCTCTGTCCTTGTAAGTCAGTTGACTTGCCGCACATCTCTTTGTGT ACTTGTACGGTACTGGCAGAAAAGTCATTTTTCAAAAGCCATAGGCTTTTCCTTGCCCTTAG CTGTAATAATGCATCTGATTTTGATTTCCTCCAGAGCTGTGTTTCTGTCCATCACCTGTGTA TTGGCCCTGTGTTTACCACTCTGGCCCACTCCTCACCCCCTTGCTCCCCTGGTCTTCTGGA GTTTGTGACATTGATTTGAAATGGATGGTGTTCTCTTGAGAGCAAGTGAGATTGTTAGAATT AAGTTCCAACTATACAGTTTTCTAACATAGCTATAAGGTCCTTGTTGCTGTTTGTGATAACTG ATAGATAACTCATTGGAAACGTGCATACATTTATATTCAGATGAAATTATGGTTTGCACTGTC TATTAAATATCTCGATTAATTTTCATA). This sequence maintains the GA rich motifs thought to be important for translocation.

To insert the various doxycycline-inducible constructs into the backbone (pRD-RIPE), we used the NEBuilder Assembly tool and followed the programs direction to generate forward and reverse primers for generating PCR products for the insert and the backbone (listed in the Table 3 below). Q5 High-Fidelity 2x Master Mix (New England Biolabs) was used to perform the PCR according to the manufacturer's protocol. NEBuilder HiFi DNA Assembly Master Mix was used to assemble the inserts and backbones according to the manufacturer's protocol and transformed into XL10-Gold competent cells (Agilent). Bacteria containing the constructs were then grown overnight at 37°C and the DNA was extracted using the Zyppy Plasmid Miniprep Kit (Zymo Research) according to the manufacturer's protocol.

For the RFP-3'UTR, RFP-CHMP4B-3'UTR were generated as described above and then using the NEBuilder system, the CHMP4B coding region was removed by PCR and re-assembled to get RFP-3'UTR construct. For the RFP-CHMP4B No Start, the RFP-CHMP4B was generated as described above and then using the NEBuilder system, the start codon was removed by PCR and re-assembled to get the RFP-CHMP4B No Start construct.

NEBuilder Primer Sequence Name	*Primer Sequence 5' to 3'*
pRD-RIPE Forward (used for RFP only)	CGGCGCCTAAACACTCAGGTGCAGGCTG
pRD-RIPE Reverse (used for RFP only)	GGCGATTCGTGGTGGCGACCGGTGGATC
RFP Forward	GGTCGCCACCACGAATCGCCACCATGGC
RFP Reverse	ACCTGAGTGTTTAGGCGCCGGTGGAGTG
pRD-RIPE Forward (used for RFP-CHMP4B)	ATCCATGTAAACACTCAGGTGCAGGCTG
pRD-RIPE Forward (used for RFP-CHMP4B)	GGCGATTCGTGGTGGCGACCGGTGGATC
RFP-CHMP4B Forward	GGTCGCCACCACGAATCGCCACCATGGC
RFP-CHMP4B Reverse	ACCTGAGTGTTTACATGGATCCAGCCCAG
pRD-RIPE Forward (used for 5'-RFP-CHMP4B)	ATCCATGTAAACACTCAGGTGCAGGCTG
pRD-RIPE Forward (used for 5'-RFP-CHMP4B)	AGGCCTCTCCGGTGGCGACCGGTGGATC
5'-RFP-CHMP4B Forward	GGTCGCCACCGGAGAGGCCTGCGGCGGC
5'-RFP-CHMP4B Reverse	ACCTGAGTGTTTACATGGATCCAGCCCAG TTATCCAATTCCTTCATGTC

pRD-RIPE Forward (used for RFP-CHMP4B-3')	ATTTTCATATACACTCAGGTGCAGGCTG
pRD-RIPE Forward (used for RFP-CHMP4B-3')	GGCGATTCGTGGTGGCGACCGGTGGATC
RFP-CHMP4B-3' Forward	GGTCGCCACCACGAATCGCCACCATGGC
RFP-CHMP4B-3' Reverse	ACCTGAGTGTATATGAAAATTAATCGAGA TATTTAATAGACAGTGCAAAC
pRD-RIPE Forward (used for 5'-RFP-CHMP4B-3')	ATTTTCATATACACTCAGGTGCAGGCTG
pRD-RIPE Forward (used for 5'-RFP-CHMP4B-3')	AGGCCTCTCCGGTGGCGACCGGTGGATC
5'-RFP-CHMP4B-3' Forward	GGTCGCCACCGGAGAGGCCTGCGGCGGC
5'-RFP-CHMP4B-3' Reverse	ACCTGAGTGTATATGAAAATTAATCGAGAT ATTTAATAGACAGTGCAAACCATAATTT
RFP-3'UTR Forward	AGATCTCGAGTAAGAATTCTGCAGTCGAC
RFP-3'UTR Reverse	AGAATTCTTACTCGAGATCTGAGTACTTG
RFP-CHMP4B No Start Forward	AATCGCCACCGCCTCCTCCGAGGACGTC
RFP-CHMP4B No Start Reverse	CGGAGGAGGCGGTGGCGATTCGTGGTGG

Transfection of doxycycline-inducible constructs

HeLa acceptor lines containing a HeLa LoxP site were plated in a 6-well plate and allowed to grow to 60% confluency. Cells were then co-transfected with a pRD-RIPE construct containing a gene of interest, along with a Cre-encoding plasmid (pBT140) at a 0.5%-10% wt/wt ratio. To transfect 1 well in a 6-well plate, a total of 2.1µg of DNA was mixed with 5.625µL of Lipofectamine 2000 (Thermo Fisher Scientific) and 246µL of Opti-MEM (Invitrogen) following the manufacturer's protocol. Cells were incubated with the transfection mixture overnight, the medium was changed, and the incubation continued for another 24 h before adding puromycin. We used a two-step selection protocol, beginning with half of the maximal puromycin concentration (0.5µg/mL) for the first 48 h of selection, followed by the maximal puromycin concentration (1µg/mL) for several days until the puromycin-sensitive cells were eliminated. The cultures were incubated until the appearance of visible puromycin-resistant colonies, which were then pooled together and expanded.

Induction of doxycycline-inducible cell lines

Cells containing a doxycycline-inducible gene of interest were subject to 2µg/mL of doxycycline and allowed to grow for 48 h unless otherwise stated. After 48 h, the cells were either fixed on collagen-coated coverslips for immunofluorescence, lysed for western blot analysis, or the media was collected for MBsome isolation.

Cell lysis and western blot analysis

Cells were lysed on ice in a buffer containing 20 mM Hepes, pH 7.4, 150 mM NaCl, 1% Triton X-100, and 1 mM PMSF. After 30 min, lysates were clarified at 15,000 g in a prechilled microcentrifuge. Supernatants were collected and analyzed via Bradford assay (5000006; Bio-Rad Protein Assay). 50-µg lysate samples were prepared (unless otherwise stated) in 4× SDS loading dye, boiled for 5 min at 95°C, and separated via SDS-PAGE. Gels were transferred onto 0.45-µm polyvinylidene difluoride membrane (IPFL00010), followed by blocking for 30 min in Intercept Blocking Buffer diluted in TBST 1:3 (927-60001). Primary antibodies (made in diluted Intercept Blocking Buffer) were incubated overnight at 4°C. The next day, blots were washed in TBST followed by incubation with IRDye fluorescent secondary

antibody (diluted Intercept Blocking Buffer) for 30 min at room temperature. Blots were washed once again with TBST before final imaging on a Li-Cor Odyssey CLx.

Statistical analysis
All statistical analyses were performed using GraphPad Prism Software (GraphPad, San Diego, CA). A Student's t-test was used to determine significance unless otherwise noted. Error bars represent standard deviation unless otherwise noted. For all immunofluorescence experiments, at least 20 randomly chosen image fields from at least 3 separate experiments were used for data collection. For quantitative immunofluorescence analysis, the same exposure was used for all images in that experiment and was quantified using Intelligent Imaging Innovations software (Denver, CO, USA). For western blot experiments, 3 separate experimental examples were used for data collection. For quantitative western blot analysis, Image Studio V5.2 software (LI-COR, Lincoln, NE) was used to collect intensities.

Acknowledgements
We would like to thank the University of Colorado Anschutz Medical Campus Genomics Facility and Novogene for performing the RNAseq and the RNA Biosciences Initiative (RBI) for help in analyzing the RNAseq data and Migle Prekeryte for critically reading and editing the manuscript. This work was supported by NIGMS grant R01-GM143774 to RP, R35-GM133385 to JMT, and RBI Pilot Grant to RP and JMT. Additionally, some of the work was also supported by Diversity Supplement GM143774-02S1 to KV.

Figure Legends
Figure 1. MBsomes contain a distinct subset of mRNAs.
(A) Schematic representing MB formation and MBsome release into the media. MBsomes from the media were isolated for RNAseq analysis presented in this study.
(B) Principal component analysis representing the difference between the 3 control and the 3 MB RNAseq datasets.
(C) Correlation analysis representing the correlation between the various control and MB RNAseq datasets.
(D) Volcano plot showing the significantly depleted (pink) and significantly enriched (purple) mRNAs found within MBsomes from 3 RNAseq datasets.

Figure 2. MBsomes are enriched in mRNAs encoding proteins that regulate translation and cell cycle.
(A) The Gene Ontology (GO) pathway analysis tool was used to determine the pathways associated with the enriched MB-associated mRNAs.
(B) MB enrichment of mRNAs encoding known abscission regulators. Data shown presents means and standard deviations derived from three separate RNAseq analyses. Dashed line marks the mRNA levels present in the whole cell transcriptome.
(C) Whole cell or MBsome-associated mRNAs were isolated from GFP-MKLP1-expressing HeLa cell line. The cDNA was subject to RT-qPCR using TSG101, CHMP4B, CHMP2A, CHMP3, CHMP6, or GAPDH (control) specific primers and represented as normalized values. Statistical analysis is represented with a p-value.
(D) Schematic representing key regulators of abscission and how they relate to each other in the intercellular bridge.

Figure 3. Midbodies contain molecular machinery required for protein translation.
(A) GFP-MKLP1 expressing HeLa cells were either mock treated or treated with CHMP4B siRNA for 72 h and subjected to staining with smFISH probes against CHMP4B. Arrows in the

inset points to CHMP4B mRNA particles. The cell outline is marked in yellow with the asterisks marking the MB. The black dashed square represents the region of the image used for the inset.
(B) ImageJ was used to count the number of CHMP4B smFISH particles in the mock or CHMP4B siRNA treated cells. Each dot represents a single cell.
(C) The Database for Annotation, Visualization, and Integrated Discovery (DAVID) was used to determine that ribosomal proteins and translation initiation factors are enriched in all 3 published MB proteomes.
(D) HeLa cells were fixed and subjected to immunostaining with anti-acetylated-tubulin (red) and anti-RPL3 (green) antibodies. The line used for the line intensity graphs is marked in yellow and the asterisks mark the MB. The white dashed square represents the region of the image used for the inset.
(E-F) Line intensity graphs representing the intensity of acetylated-tubulin (red) and RPL3 (green). Negative control was derived from samples that were treated with secondary antibodies but without anti-RPL3 antibodies.

Figure 4. Active protein translation occurs in the midbody.
(A) Schematic representing the 3 treatment conditions and times used for the experiments represented in panels (B-E).
(B) HeLa cells were treated with either DMSO, CHX+Puromycin, or Puromycin and subjected to immunostaining with anti-acetylated-tubulin and anti-puromycin antibodies. The asterisks mark the MB, and the white dashed square represents the region of the image used for the inset.
(C-D) 3i imaging software was used to measure the anti-puromycin intensity/micron^2 in the intercellular bridge of 60 cells from 3 separate experiments (C; each dot represents one cell). Statistical analysis was done on means and standard deviations derived from the 3 individual experiments (D). Each experiment is represented by a different shade of color and is the mean derived from all cells analyzed in that particular experiment. Statistical analysis is represented with a p-value.
(E) HeLa cells were treated with either DMSO, CHX+Puromycin, or Puromycin and subjected to immunostaining with anti-puromycin (to mark the puromycylated peptides) and anti-CHMP4B antibodies. The line used for the line intensity graphs is marked in yellow and the asterisks mark the MB. The white dashed square represents the region of the image used for the inset.
(F-H) Line intensity graphs representing the intensity of Puromycin (red) and CHMP4B (green) signals after DMSO (F), CHX+Puromycin (G), or Puromycin (H) treatments.

Figure 5. Inhibition of translation inhibits CHMP4B accumulation at the midbody.
(A) HeLa cells were either untreated or treated with puromycin for 1 h and subjected to immunostaining with anti-acetylated-tubulin and anti-CHMP4B antibodies. The asterisks mark the MB, and the white dashed square represents the region of the image used for the inset.
(B-C) Shown data represents CHMP4B intensity/micron^2 in the intercellular bridge of 60 cells from 3 separate experiments. Panel B shows distributions derived from individual cells (each dot represents a single cell). Statistical analysis in panel C was done on the means and standard deviations derived from the 3 individual experiments where experimental means were calculated by averaging values from all the cells from each experiment. Each experiment is represented by a different shade of color. Statistical analysis is represented with a p-value.
(D-E) Shown data represents CHMP4B intensity/micron^2 in the cell body of 60 cells from 3 separate experiments. Panel D shows distributions derived from individual cells (each dot represents a single cell). Statistical analysis in panel E was done on the means, and standard deviations were derived from the 3 individual experiments where experimental means were calculated by averaging values from all the cells from each experiment. Each experiment is represented by a different shade of color. Statistical analysis is represented with a p-value.

(F) HeLa cells were either untreated or treated with puromycin for 1 h and subjected to immunostaining with anti-acetylated-tubulin and anti-CEP55 antibodies. The asterisks mark the MB, and the white dashed square represents the region of the image used for the inset.
(G-H) Shown data represents CEP55 intensity/micron^2 in the intercellular bridge of 60 cells from 3 separate experiments. Panel G shows distributions derived from individual cells (each dot represents a single cell). Statistical analysis in panel H was done on the means, and standard deviations were derived from the 3 individual experiments where experimental means were calculated by averaging values from all the cells from each experiment. Each experiment is represented by a different shade of color. Statistical analysis is represented with a p-value.
(I-J) Shown data represents CEP55 intensity/micron^2 in the cell body of 60 cells from 3 separate experiments. Panel I show the distributions derived from individual cells (each dot represents a single cell). Statistical analysis in panel J was done on the means, and standard deviations were derived from the 3 individual experiments where experimental means were calculated by averaging values from all the cells from each experiment. Each experiment is represented by a different shade of color. Statistical analysis is represented with a p-value.
(K) HeLa cells after puromycin treatment were fixed and stained with anti-acetylated tubulin antibodies. The percentage of cells in telophase was then counted. Shown data are the means and standard deviations derived from three independent experiments. Statistical analysis is represented with a p-value.
(L) HeLa cells after puromycin treatment were fixed and stained with anti-acetylated tubulin antibodies. The percentage of cells that just completed abscission was then counted. Shown data are the means and standard deviations derived from three independent experiments. Statistical analysis is represented with a p-value.
(M) HeLa cells were either untreated, treated with puromycin, CEP55 siRNA, or CEP55 siRNA plus puromycin and subjected to immunostaining anti-acetylated-tubulin and anti-CHMP4B antibodies. The asterisks mark the MB, and the white dashed square represents the region of the image used for the inset.
(N-O) Shown data represents CHMP4B intensity/micron^2 in intracellular of 60 cells from 3 separate experiments. Panel N shows distributions derived from individual cells (each dot represents a single cell). Statistical analysis in panel O was done on the means, and standard deviations were derived from the 3 individual experiments where experimental means were calculated by averaging values from all the cells from each experiment. Each experiment is represented by a different shade of color. Statistical analysis is represented with a p-value.

Figure 6. Puromycin wash-out leads to fast recovery of CHMP4B levels in MB.
(A) HeLa cells were either untreated or treated for 1 h with puromycin. Cells were then washed and incubated with complete media for either 5 min or 10 min. Cells were then fixed and subjected to immunostaining with anti-acetylated-tubulin and anti-CHMP4B antibodies. The asterisks mark the MB, and the white dashed square represents the region of the image used for the inset.
(B-C) Shown data represents CHMP4B intensity/micron^2 in the intercellular bridge of 60 cells from 3 separate experiments. Panel B shows distributions derived from individual cells (each dot represents a single cell). Statistical analysis in panel C was done on the means, and standard deviations were derived from the 3 individual experiments where experimental means were calculated by averaging values from all the cells from each experiment. Each experiment is represented by a different shade of color. Statistical analysis is represented with a p-value.
(D-E) Shown data represents CHMP4B intensity/micron^2 in the cell body of 60 cells from 3 separate experiments. Panel D shows distributions derived from individual cells (each dot represents a single cell). Statistical analysis in panel E was done on the means, and standard deviations were derived from the 3 individual experiments where experimental means were

calculated by averaging values from all the cells from each experiment. Each experiment is represented by a different shade of color. Statistical analysis is represented with a p-value.
(F-G) HeLa cells that were untreated or treated for 1 h with puromycin. Cells were then washed and incubated with media for an additional 5 or 10 minutes. Cells were then fixed and stained with anti-acetylated-tubulin antibodies. The percentage of cells in either telophase (F) or just after abscission (G) was then counted. Shown data are means and standard deviations derived from three independent experiments. Statistical analysis is represented with a p-value.

Figure 7. The 3'UTR of CHMP4B is important for protein accumulation and mRNA translocation.
(A) HeLa cells expressing various RFP-tagged dox-inducible constructs were incubated with 2μg/mL doxycycline for 48 h and then subjected to immunostaining with anti-acetylated-tubulin. The asterisks mark the MB, and the white dashed square represents the region of the image used for the inset.
(B-C) Ratio between RFP fluorescence in the intracellular bridge and cell body was calculated from 60 randomly chosen cells in telophase. Panel B shows distributions derived from individual cells (each dot represents a single cell). Statistical analysis in panel C was done on the means, and standard deviations were derived from the 3 individual experiments where experimental means were calculated by averaging values from all the cells from each experiment. Each experiment is represented by a different shade of color. Statistical analysis is represented with a p-value.
(D) HeLa cells expressing various RFP-tagged dox-inducible constructs were incubated with 2μg/mL doxycycline for 48 h and then subjected to immunostaining with anti-acetylated-tubulin. The percentage of cells with multinucleation was then counted. Shown data are the means and standard deviations derived from three independent experiments. Statistical analysis is represented with a p-value.
(E) HeLa cells expressing various RFP-tagged dox-inducible constructs were incubated with 2μg/mL doxycycline for 48 h and then subjected to immunostaining with anti-acetylated-tubulin. The percentage of cells in telophase was then counted. Shown data are the means and standard deviations derived from three independent experiments. Statistical analysis is represented with a p-value.
(F) HeLa cells expressing dox-inducible RFP-CHMP4B or RFP-CHMP4B-3'UTR constructs were incubated with 2μg/mL doxycycline for 48 h and subjected to staining with smFISH probes against CHMP4B. The cell outline is marked in yellow with the asterisks marking the MB. The black dashed square represents the region of the image used for the inset.
(G) Whole cell or MB-associated mRNA was isolated from these cell lines expressing various RFP-tagged constructs and subject to RT-qPCR analysis using RFP or GAPDH (control) specific primers. RFP mRNA levels were then normalized against GAPDH mRNA and expressed as a ratio between MB and whole cell RFP mRNA levels. Statistical analysis is represented with a p-value and was done on the means and standard deviations derived from three independent experiments.

Supplemental Figure 1. CHMP4B and CEP55 KD validation via RT-qPCR.
GFP-MKLP1 expressing HeLa cells were either mock treated or treated with CHMP4B (A) or CEP55 (B) siRNAs. Cells were then incubated for 72 h, followed by mRNA isolation and RT-qPCR analysis using CHMP4B, CEP55, and GAPDH (control) specific primers. Data shown are the CHMP4B or CEP55 mRNA levels normalized against GAPDH mRNA.

Supplemental Figure 2. CHMP4B mRNA targeting to MB is not dependent on translation.

GFP-MKLP1 expressing HeLa cells were either mock treated (top two panels) or treated with puromycin for 1 h (bottom two panels) and subject to staining with smFISH probes against CHMP4B mRNA. CHMP4B mRNA particles are marked by the arrows in the inset and the black dashed square represents the region of the image used for the inset (A). The number of cells with CHMP4B smFISH signal was then counted. The data shown in panel B represents the means and standard deviations derived from three independent experiments.

Supplemental Figure 3. Identification of cells that have just undergone abscission.
(A-B) HeLa cells were fixed and subjected to immunostaining using anti-acetylated-tubulin. The panel A represents a cell in telophase. Panel B represents a cell that had just undergone abscission (see arrow). The lines used for the line intensity graphs are marked in yellow, and the white dashed square represents the region of the image used for the inset.
(C-D) Line intensity graphs representing the intensity of acetylated-tubulin in telophase and abscission cells. The abscission site is marked by an arrow (D).

Supplemental Figure 4. Characterization of HeLa LoxP cells expressing doxycycline-inducible RFP-tagged constructs.
(A) HeLa LoxP cells expressing various RFP-tagged dox-inducible constructs cells were untreated (-Dox) or treated with 2μg/mL doxycycline for 48 h (+Dox). RFP was visualized by fluorescent microscopy to test for dox-dependent expression. The white dashed square represents the region of the image used for the inset.
(B-D) HeLa LoxP cells expressing various RFP-tagged dox-inducible constructs cells were untreated (-Dox) or treated with 2μg/mL doxycycline for 48 h (+Dox). The construct expression levels were then determined by RT-qPCR using CHMP4B specific primers.
(E) HeLa LoxP cells expressing various RFP-tagged dox-inducible constructs cells were treated with 2μg/mL doxycycline for 48 h. The levels of expression among various constructs were the n compared using RT-qPCR with RFP specific primers.
(F-G) HeLa LoxP cells expressing various RFP-tagged dox-inducible constructs cells were untreated (-Dox) or treated with 2μg/mL doxycycline for 48 h (+Dox). The levels of RFP-tagged protein expressions were visualized via western blot using anti-RFP and anti-Actin (loading control) antibodies. Panel G shows Western blot quantification from 3 individual experiments. Statistical analysis is represented with a p-value.

Supplemental Table 4. List of mRNAs identified in RNAseq analyses of purified MBs

References

1. Carlton, J. The ESCRT machinery: a cellular apparatus for sorting and scission. *Biochem Soc Trans* **38**, 1397-1412 (2010).
2. Schoneberg, J., Lee, I.H., Iwasa, J.H. & Hurley, J.H. Reverse-topology membrane scission by the ESCRT proteins. *Nat Rev Mol Cell Biol* **18**, 5-17 (2017).
3. Carlton, J.G. & Martin-Serrano, J. Parallels between cytokinesis and retroviral budding: a role for the ESCRT machinery. *Science* **316**, 1908-1912 (2007).
4. Morita, E. *et al.* Human ESCRT and ALIX proteins interact with proteins of the midbody and function in cytokinesis. *EMBO J* **26**, 4215-4227 (2007).

5. Carlton, J.G., Agromayor, M. & Martin-Serrano, J. Differential requirements for Alix and ESCRT-III in cytokinesis and HIV-1 release. *Proc Natl Acad Sci U S A* **105**, 10541-10546 (2008).
6. Guizetti, J. *et al.* Cortical constriction during abscission involves helices of ESCRT-III-dependent filaments. *Science* **331**, 1616-1620 (2011).
7. Goliand, I., Nachmias, D., Gershony, O. & Elia, N. Inhibition of ESCRT-II-CHMP6 interactions impedes cytokinetic abscission and leads to cell death. *Mol Biol Cell* **25**, 3740-3748 (2014).
8. Addi, C. *et al.* The Flemmingsome reveals an ESCRT-to-membrane coupling via ALIX/syntenin/syndecan-4 required for completion of cytokinesis. *Nat Commun* **11**, 1941 (2020).
9. Elia, N., Sougrat, R., Spurlin, T.A., Hurley, J.H. & Lippincott-Schwartz, J. Dynamics of endosomal sorting complex required for transport (ESCRT) machinery during cytokinesis and its role in abscission. *Proc Natl Acad Sci U S A* **108**, 4846-4851 (2011).
10. Goliand, I. *et al.* Resolving ESCRT-III Spirals at the Intercellular Bridge of Dividing Cells Using 3D STORM. *Cell Rep* **24**, 1756-1764 (2018).
11. Christ, L., Raiborg, C., Wenzel, E.M., Campsteijn, C. & Stenmark, H. Cellular Functions and Molecular Mechanisms of the ESCRT Membrane-Scission Machinery. *Trends Biochem Sci* **42**, 42-56 (2017).
12. Agromayor, M. *et al.* Essential role of hIST1 in cytokinesis. *Mol Biol Cell* **20**, 1374-1387 (2009).
13. Christ, L. *et al.* ALIX and ESCRT-I/II function as parallel ESCRT-III recruiters in cytokinetic abscission. *J Cell Biol* **212**, 499-513 (2016).
14. Morita, E. *et al.* Human ESCRT-III and VPS4 proteins are required for centrosome and spindle maintenance. *Proc Natl Acad Sci U S A* **107**, 12889-12894 (2010).
15. Carlton, J.G., Caballe, A., Agromayor, M., Kloc, M. & Martin-Serrano, J. ESCRT-III governs the Aurora B-mediated abscission checkpoint through CHMP4C. *Science* **336**, 220-225 (2012).
16. Mierzwa, B. & Gerlich, D.W. Cytokinetic abscission: molecular mechanisms and temporal control. *Dev Cell* **31**, 525-538 (2014).
17. Addi, C., Bai, J. & Echard, A. Actin, microtubule, septin and ESCRT filament remodeling during late steps of cytokinesis. *Curr Opin Cell Biol* **50**, 27-34 (2018).
18. Tedeschi, A. *et al.* Cep55 promotes cytokinesis of neural progenitors but is dispensable for most mammalian cell divisions. *Nat Commun* **11**, 1746 (2020).
19. Dionne, L.K., Wang, X.J. & Prekeris, R. Midbody: from cellular junk to regulator of cell polarity and cell fate. *Curr Opin Cell Biol* **35**, 51-58 (2015).
20. Kuo, T.C. *et al.* Midbody accumulation through evasion of autophagy contributes to cellular reprogramming and tumorigenicity. *Nat Cell Biol* **13**, 1214-1223 (2011).
21. Crowell, E.F., Gaffuri, A.L., Gayraud-Morel, B., Tajbakhsh, S. & Echard, A. Engulfment of the midbody remnant after cytokinesis in mammalian cells. *J Cell Sci* **127**, 3840-3851 (2014).
22. Chen, C.T., Ettinger, A.W., Huttner, W.B. & Doxsey, S.J. Resurrecting remnants: the lives of post-mitotic midbodies. *Trends Cell Biol* **23**, 118-128 (2013).

23. Peterman, E. *et al.* The post-abscission midbody is an intracellular signaling organelle that regulates cell proliferation. *Nat Commun* **10**, 3181 (2019).
24. Rai, A. *et al.* Secreted midbody remnants are a class of extracellular vesicles molecularly distinct from exosomes and microparticles. *Commun Biol* **4**, 400 (2021).
25. Skop, A.R., Liu, H., Yates, J., 3rd, Meyer, B.J. & Heald, R. Dissection of the mammalian midbody proteome reveals conserved cytokinesis mechanisms. *Science* **305**, 61-66 (2004).
26. Peterman, E. & Prekeris, R. Understanding post-mitotic roles of the midbody during cell differentiation and polarization. *Methods Cell Biol* **137**, 173-186 (2017).
27. Tsanov, N. *et al.* smiFISH and FISH-quant - a flexible single RNA detection approach with super-resolution capability. *Nucleic Acids Res* **44**, e165 (2016).
28. Holt, C.E. & Bullock, S.L. Subcellular mRNA localization in animal cells and why it matters. *Science* **326**, 1212-1216 (2009).
29. Khandelia, P., Yap, K. & Makeyev, E.V. Streamlined platform for short hairpin RNA interference and transgenesis in cultured mammalian cells. *Proc Natl Acad Sci U S A* **108**, 12799-12804 (2011).
30. D'Avino, P.P. & Capalbo, L. Regulation of midbody formation and function by mitotic kinases. *Semin Cell Dev Biol* **53**, 57-63 (2016).
31. Antanaviciute, I., Gibieza, P., Prekeris, R. & Skeberdis, V.A. Midbody: From the Regulator of Cytokinesis to Postmitotic Signaling Organelle. *Medicina (Kaunas)* **54** (2018).
32. Peterman, E. & Prekeris, R. The postmitotic midbody: Regulating polarity, stemness, and proliferation. *J Cell Biol* **218**, 3903-3911 (2019).
33. Steigemann, P. & Gerlich, D.W. Cytokinetic abscission: cellular dynamics at the midbody. *Trends Cell Biol* **19**, 606-616 (2009).
34. Farmer, T. & Prekeris, R. New signaling kid on the block: the role of the postmitotic midbody in polarity, stemness, and proliferation. *Mol Biol Cell* **33** (2022).
35. Schiel, J.A. *et al.* Endocytic membrane fusion and buckling-induced microtubule severing mediate cell abscission. *J Cell Sci* **124**, 1411-1424 (2011).
36. Elad, N., Abramovitch, S., Sabanay, H. & Medalia, O. Microtubule organization in the final stages of cytokinesis as revealed by cryo-electron tomography. *J Cell Sci* **124**, 207-215 (2011).
37. Costa, G., Bradbury, J.J., Tarannum, N. & Herbert, S.P. RAB13 mRNA compartmentalisation spatially orients tissue morphogenesis. *EMBO J* **39**, e106003 (2020).
38. Moissoglu, K. *et al.* RNA localization and co-translational interactions control RAB13 GTPase function and cell migration. *EMBO J* **39**, e104958 (2020).
39. Arora, A. *et al.* High-throughput identification of RNA localization elements in neuronal cells. *Nucleic Acids Res* (2022).
40. Goering, R., Arora, A. & Taliaferro, J.M. RNA localization mechanisms transcend cell morphology. *bioRxiv*, 2022.2004.2014.488401 (2022).
41. Montagne, C. & Gonzalez-Gaitan, M. Sara endosomes and the asymmetric division of intestinal stem cells. *Development* **141**, 2014-2023 (2014).
42. Patro, R., Duggal, G., Love, M.I., Irizarry, R.A. & Kingsford, C. Salmon provides fast and bias-aware quantification of transcript expression. *Nat Methods* **14**, 417-419 (2017).

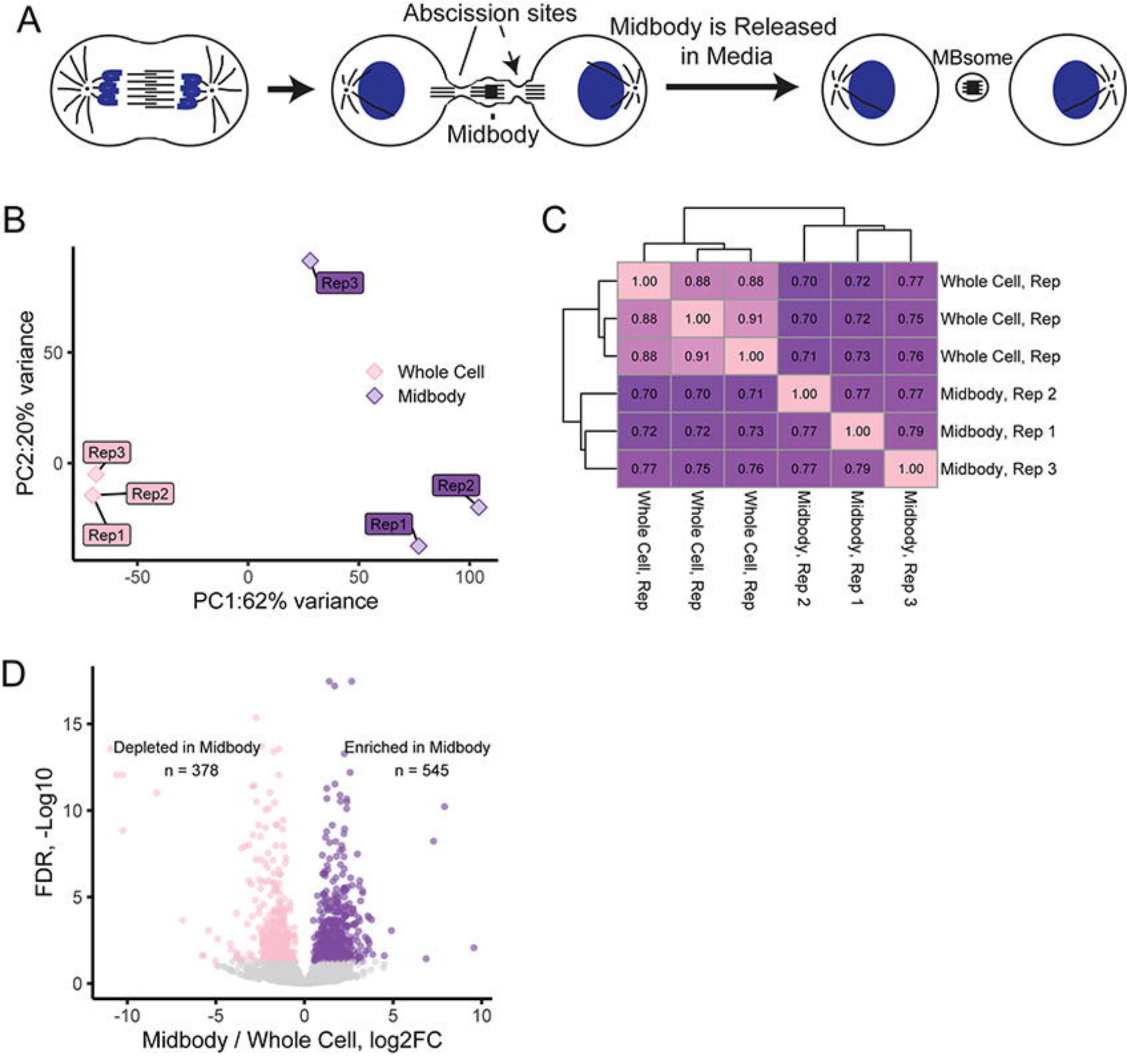
A
Abscission sites
Midbody
Midbody is Released in Media
MBsome
B
Rep3
Rep2
Rep1
Whole Cell
Midbody
PC2:20% variance
PC1:62% variance
C
1.00 0.88 0.88 0.70 0.72 0.77 Whole Cell, Rep
0.88 1.00 0.91 0.70 0.72 0.75 Whole Cell, Rep
0.88 0.91 1.00 0.71 0.73 0.76 Whole Cell, Rep
0.70 0.70 0.71 1.00 0.77 0.77 Midbody, Rep 2
0.72 0.72 0.73 0.77 1.00 0.79 Midbody, Rep 1
0.77 0.75 0.76 0.77 0.79 1.00 Midbody, Rep 3
Whole Cell, Rep
Whole Cell, Rep
Whole Cell, Rep
Midbody, Rep 2
Midbody, Rep 1
Midbody, Rep 3
D
Depleted in Midbody
n = 378
Enriched in Midbody
n = 545
FDR, -Log10
Midbody / Whole Cell, log2FC

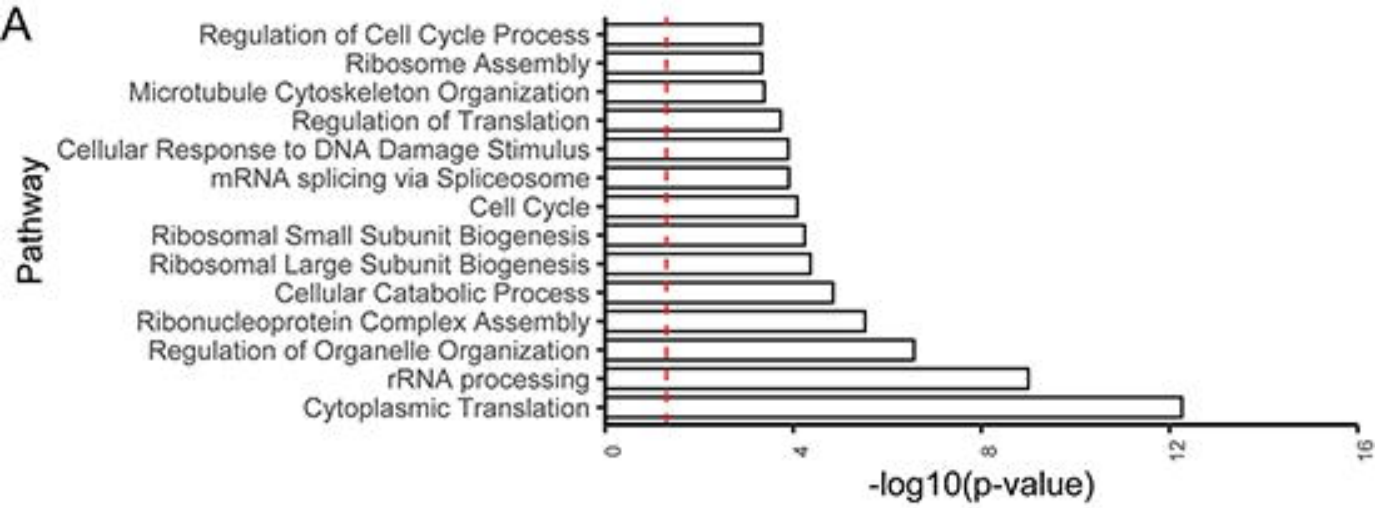
A
Pathway
Regulation of Cell Cycle Process
Ribosome Assembly
Microtubule Cytoskeleton Organization
Regulation of Translation
Cellular Response to DNA Damage Stimulus
mRNA splicing via Spliceosome
Cell Cycle
Ribosomal Small Subunit Biogenesis
Ribosomal Large Subunit Biogenesis
Cellular Catabolic Process
Ribonucleoprotein Complex Assembly
Regulation of Organelle Organization
rRNA processing
Cytoplasmic Translation
0
4
8
12
16
-log10(p-value)

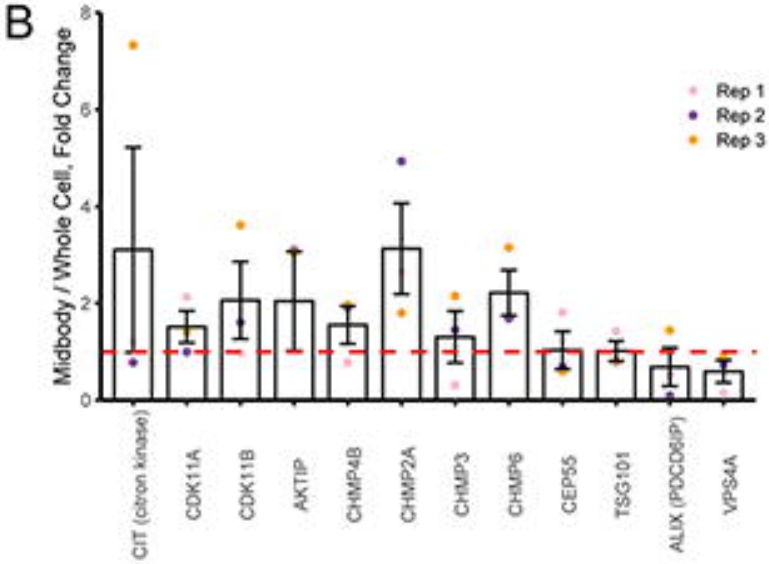
B
Midbody / Whole Cell, Fold Change
0
2
4
6
8
Rep 1
Rep 2
Rep 3
CIT (citron kinase)
CDK11A
CDK11B
AKTIP
CHMP4B
CHMP2A
CHMP3
CHMP6
CEP55
TSG101
ALIX (PDCD6IP)
VPS4A

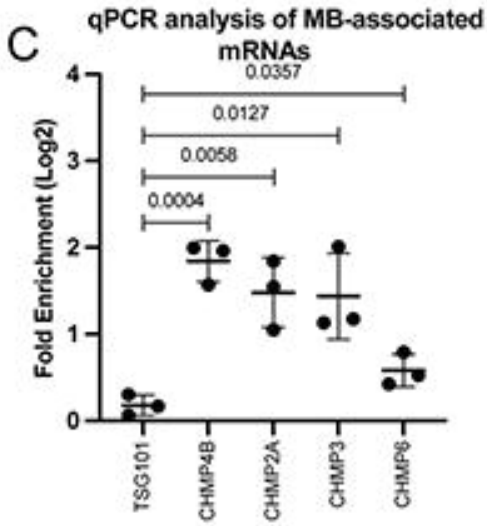
C
qPCR analysis of MB-associated mRNAs
Fold Enrichment (Log2)
0
1
2
3
4
0.0357
0.0127
0.0058
0.0004
TSG101
CHMP4B
CHMP2A
CHMP3
CHMP6

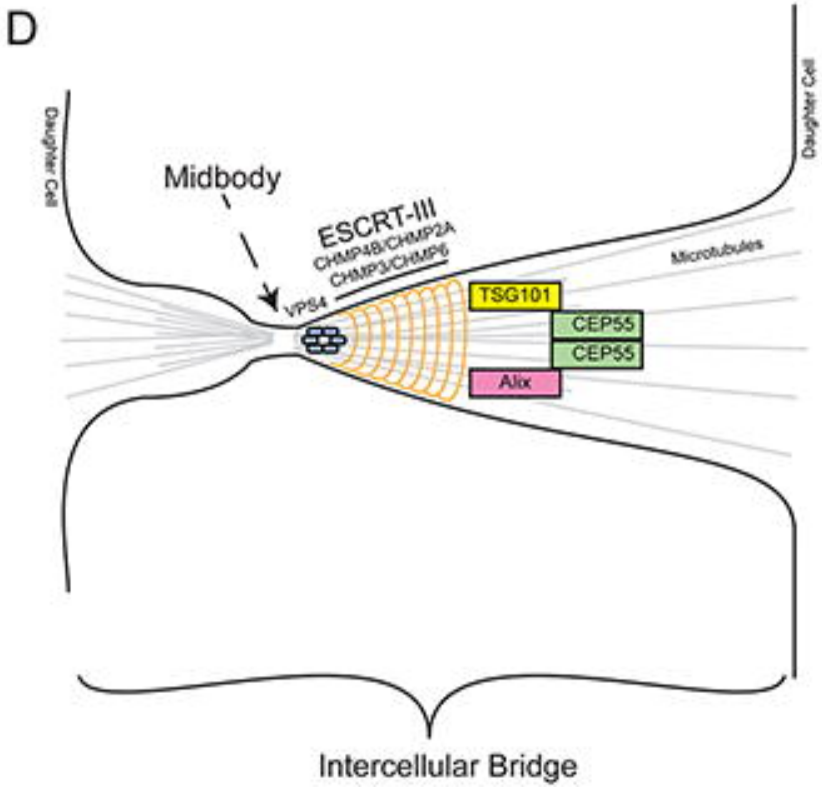
D
Daughter Cell
Daughter Cell
Midbody
ESCRT-III
CHMP4B/CHMP2A
CHMP3/CHMP6
VPS4
Microtubules
TSG101
CEP55
CEP55
Alix
Intercellular Bridge

A

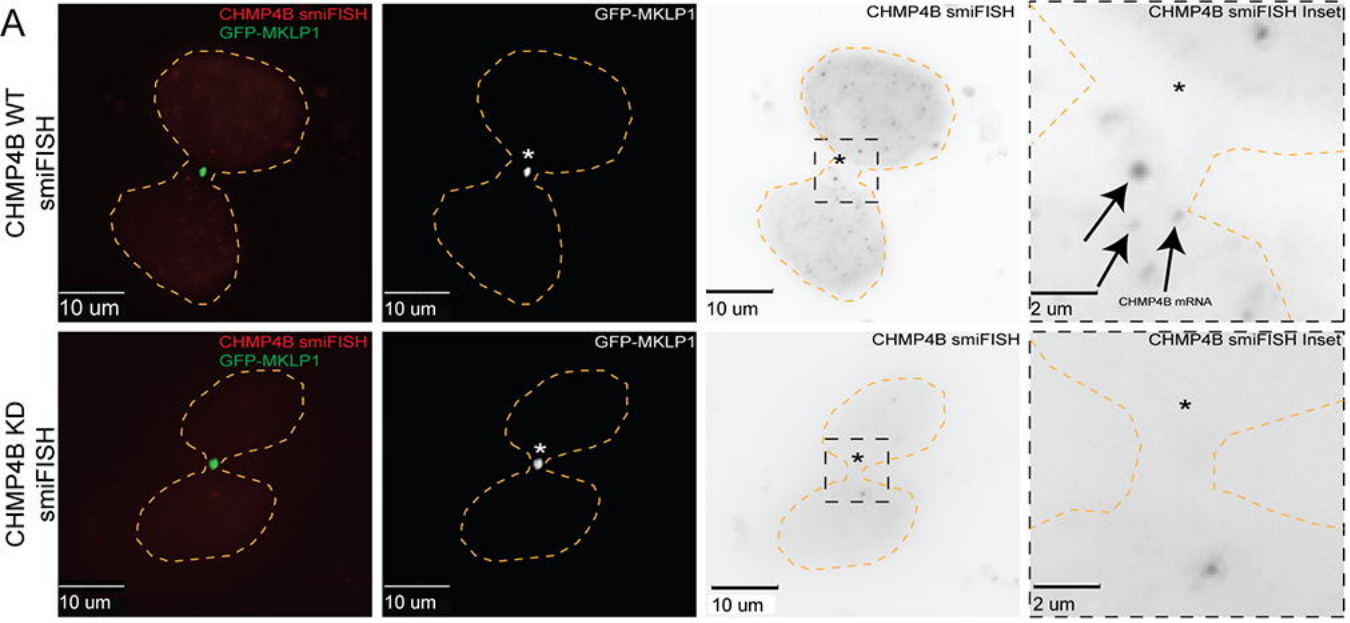

B

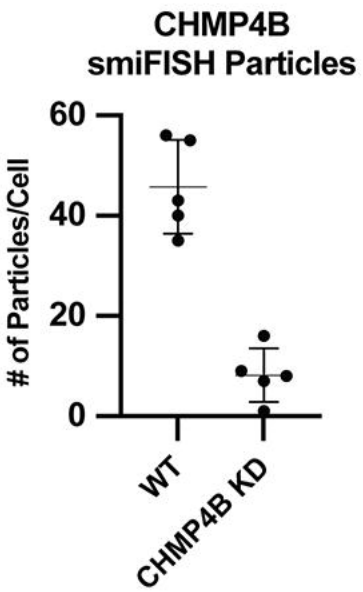

C

Ribosomal and initiation protein enrichment in the MB

Category	Data set	Enrichment Score	Citation
Ribosomal Proteins	Prekeris Lab	70.85	23
	Simpson Lab	54.95	24
	Echard Lab	80.71	8
Translation Initiation Factors	Prekeris Lab	49.07	23
	Simpson Lab	38.73	24
	Echard Lab	80.4	8

D

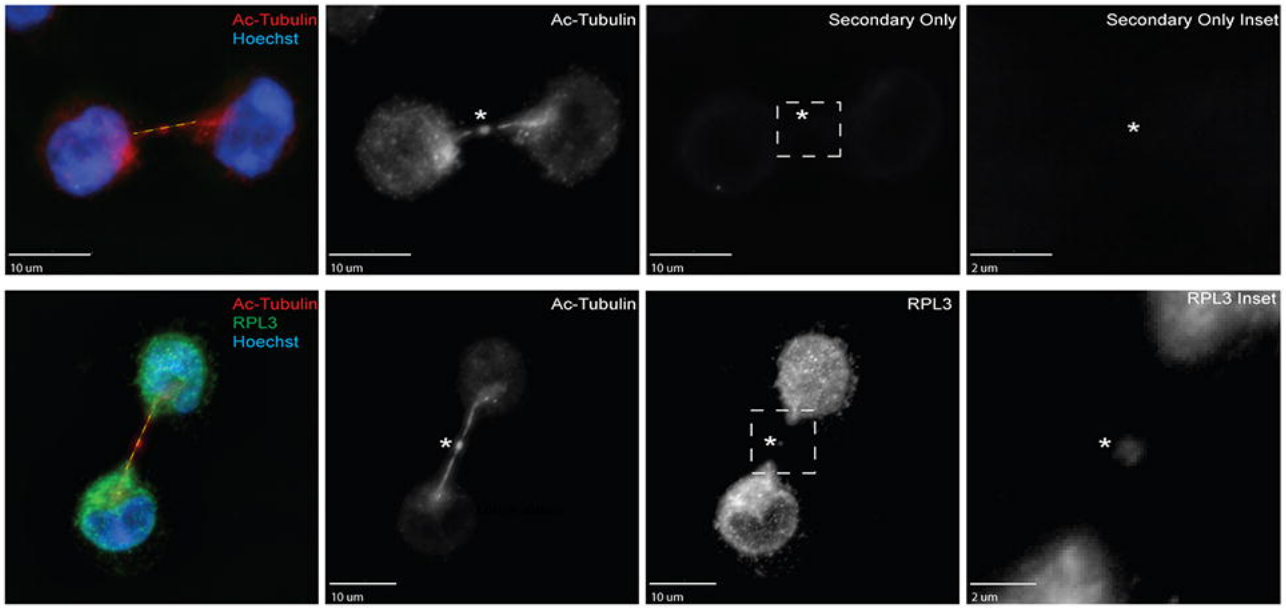

E

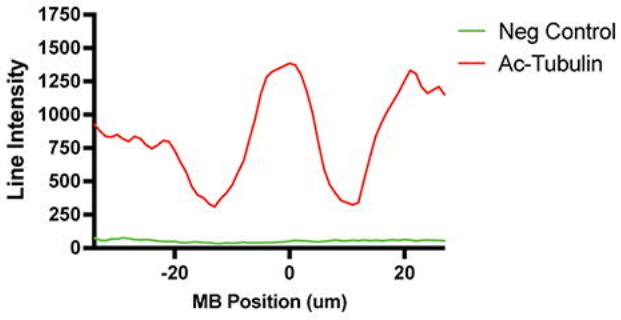

F

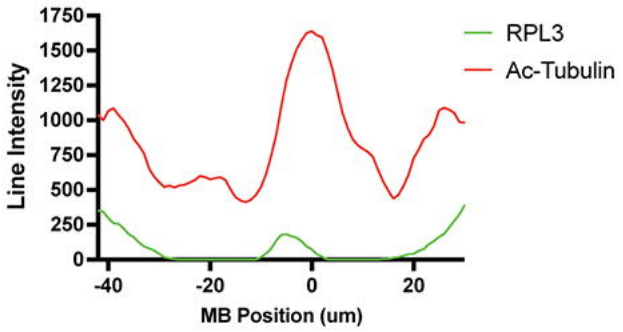

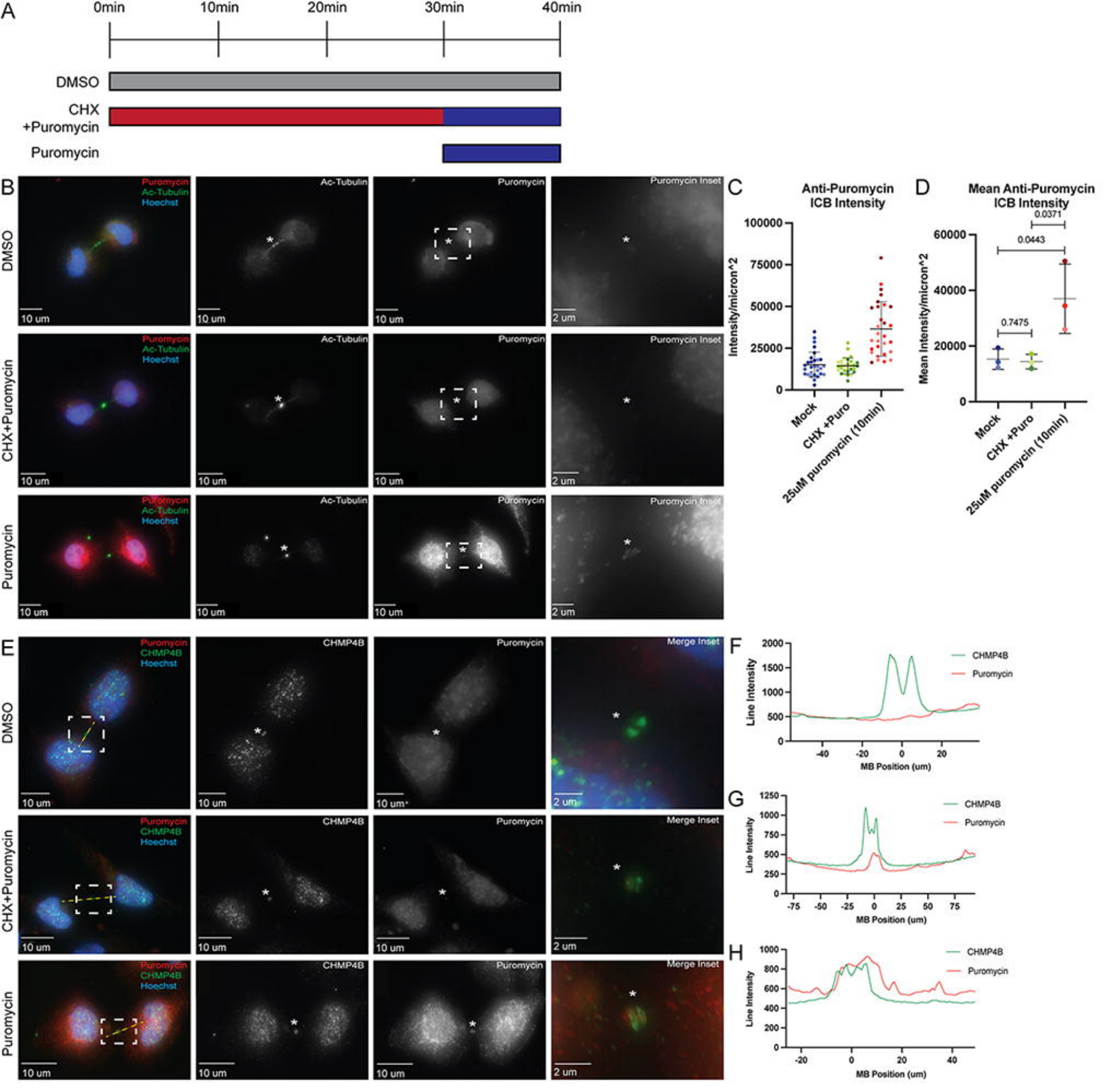
A
0min
10min
20min
30min
40min
DMSO
CHX +Puromycin
Puromycin
B
DMSO
CHX+Puromycin
Puromycin
Puromycin
Ac-Tubulin
Hoechst
Ac-Tubulin
Puromycin
Puromycin Inset
10 um
2 um
C
Anti-Puromycin ICB Intensity
Intensity/micron^2
100000
75000
50000
25000
0
Mock
CHX +Puro
25uM puromycin (10min)
D
Mean Anti-Puromycin ICB Intensity
Mean Intensity/micron^2
60000
40000
20000
0
0.0371
0.0443
0.7475
Mock
CHX +Puro
25uM puromycin (10min)
E
DMSO
CHX+Puromycin
Puromycin
Puromycin
CHMP4B
Hoechst
CHMP4B
Puromycin
Merge Inset
10 um
2 um
F
Line Intensity
MB Position (um)
CHMP4B
Puromycin
G
Line Intensity
MB Position (um)
CHMP4B
Puromycin
H
Line Intensity
MB Position (um)
CHMP4B
Puromycin

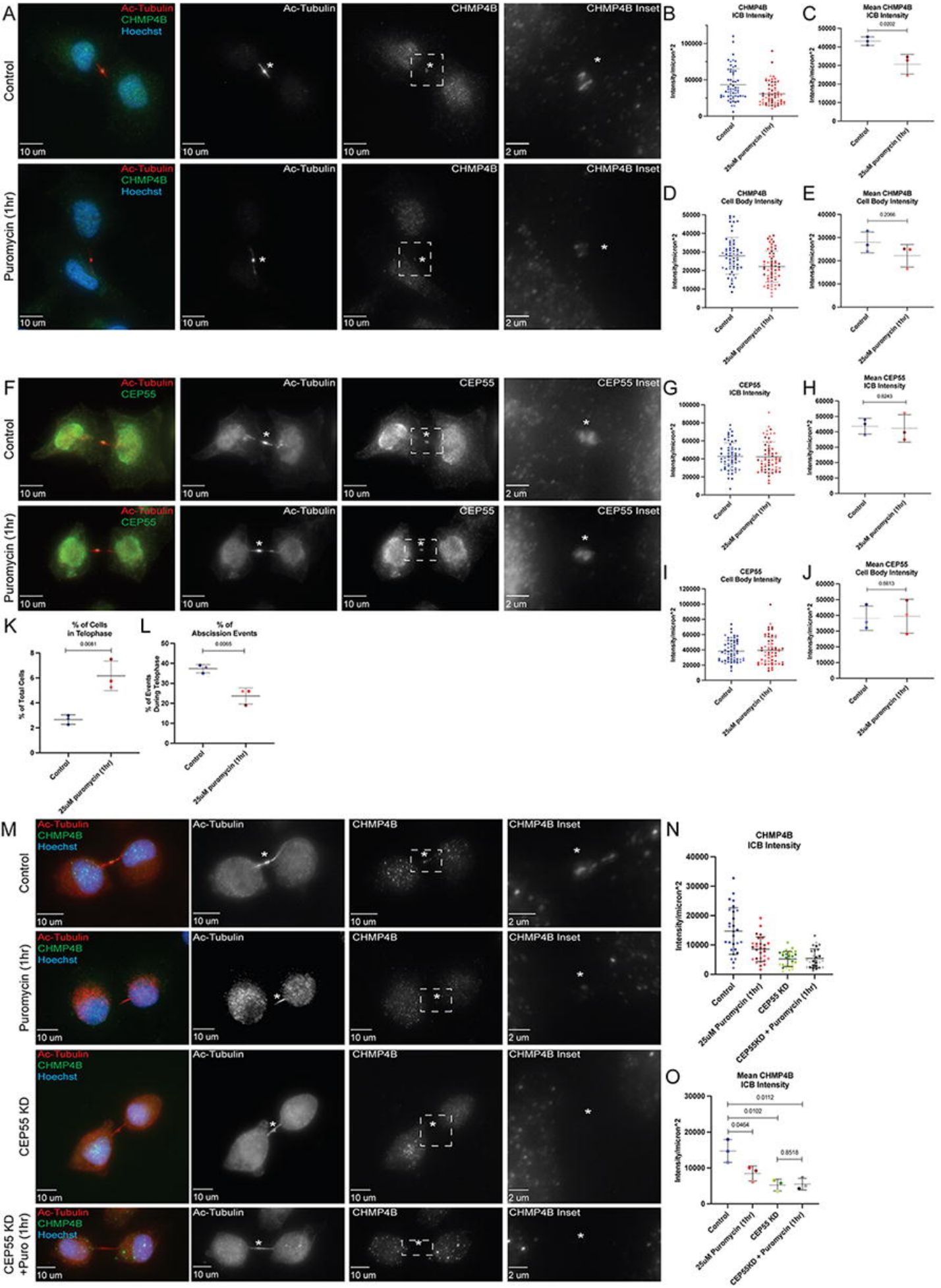
A
Ac-Tubulin
CHMP4B
Hoechst
Control
Puromycin (1hr)
Ac-Tubulin
CHMP4B
CHMP4B Inset
10 um
2 um
B
CHMP4B ICB Intensity
C
Mean CHMP4B ICB Intensity
D
CHMP4B Cell Body Intensity
E
Mean CHMP4B Cell Body Intensity
F
CEP55
CEP55 Inset
G
CEP55 ICB Intensity
H
Mean CEP55 ICB Intensity
I
CEP55 Cell Body Intensity
J
Mean CEP55 Cell Body Intensity
K
% of Cells in Telophase
% of Total Cells
L
% of Abscission Events
% of Events During Telophase
Control
25uM puromycin (1hr)
M
CEP55 KD
CEP55 KD +Puro (1hr)
N
CHMP4B ICB Intensity
Intensity/micron^2
Control
25uM Puromycin (1hr)
CEP55 KD
CEP55KD + Puromycin (1hr)
O
Mean CHMP4B ICB Intensity
0.0112
0.0102
0.0464
0.8518

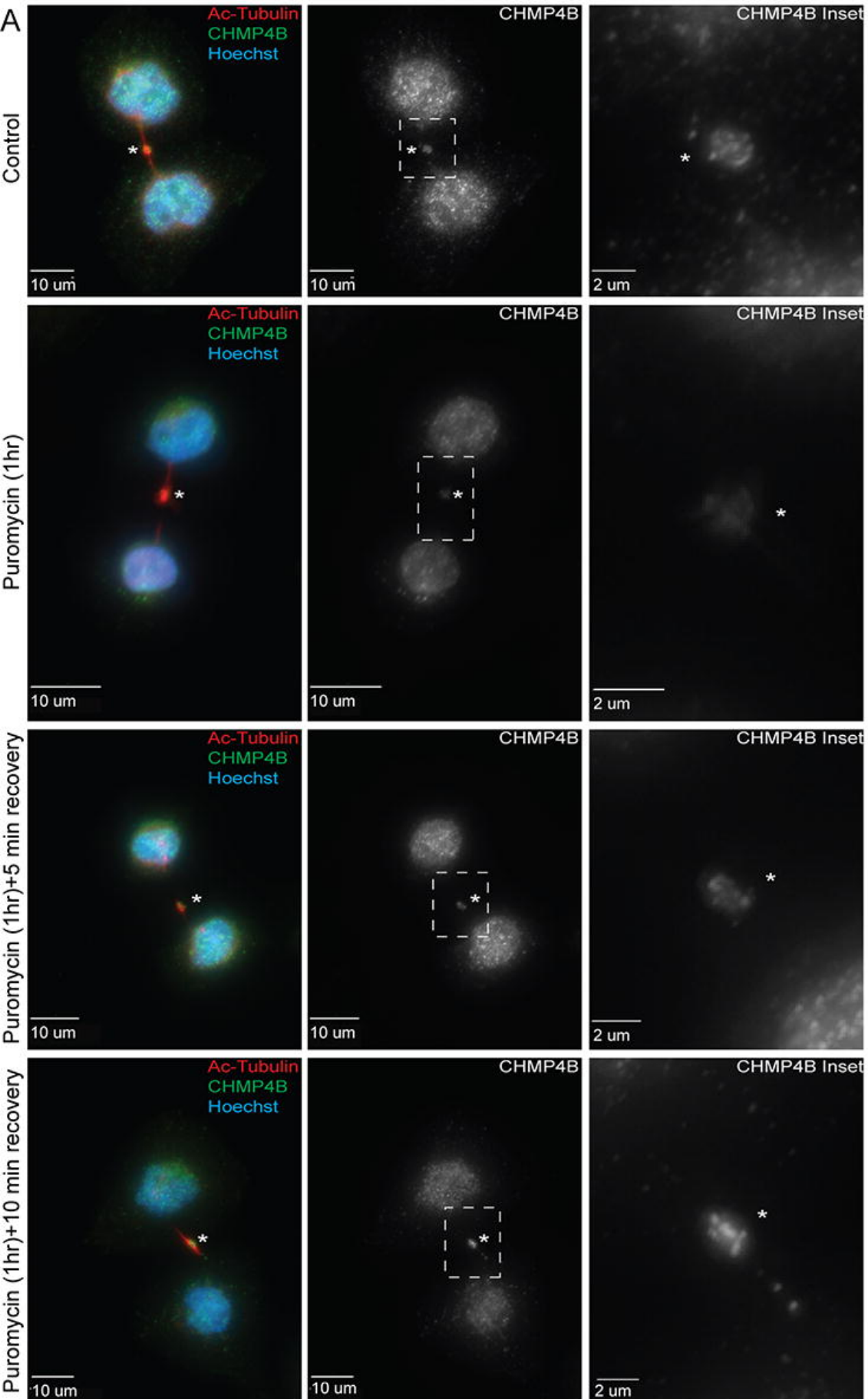
A
Ac-Tubulin
CHMP4B
Hoechst
CHMP4B
CHMP4B Inset
Control
Puromycin (1hr)
Puromycin (1hr)+5 min recovery
Puromycin (1hr)+10 min recovery
10 um
2 um

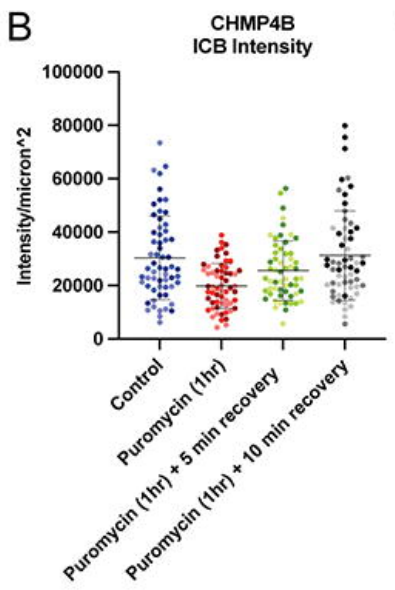
B
CHMP4B
ICB Intensity
Intensity/micron^2
100000
80000
60000
40000
20000
0
Control
Puromycin (1hr)
Puromycin (1hr) + 5 min recovery
Puromycin (1hr) + 10 min recovery

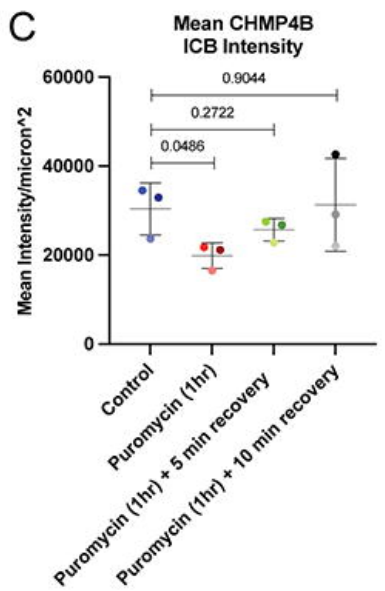
C
Mean CHMP4B
ICB Intensity
Mean Intensity/micron^2
60000
40000
20000
0
0.9044
0.2722
0.0486
Control
Puromycin (1hr)
Puromycin (1hr) + 5 min recovery
Puromycin (1hr) + 10 min recovery

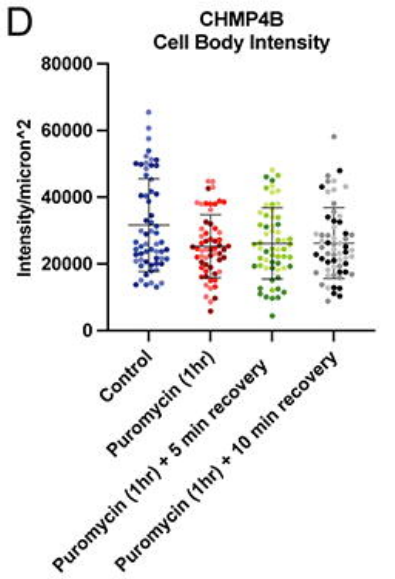
D
CHMP4B
Cell Body Intensity
Intensity/micron^2
80000
60000
40000
20000
0
Control
Puromycin (1hr)
Puromycin (1hr) + 5 min recovery
Puromycin (1hr) + 10 min recovery

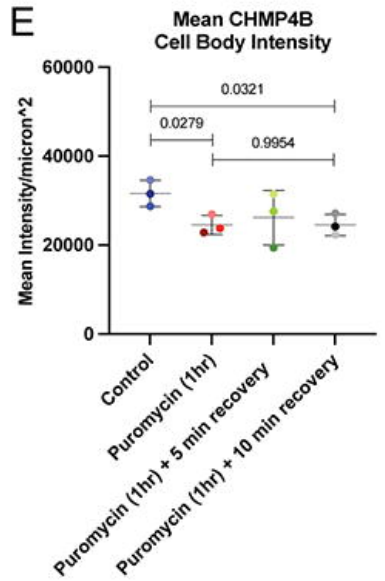
E
Mean CHMP4B
Cell Body Intensity
Mean Intensity/micron^2
60000
40000
20000
0
0.0321
0.0279
0.9954
Control
Puromycin (1hr)
Puromycin (1hr) + 5 min recovery
Puromycin (1hr) + 10 min recovery

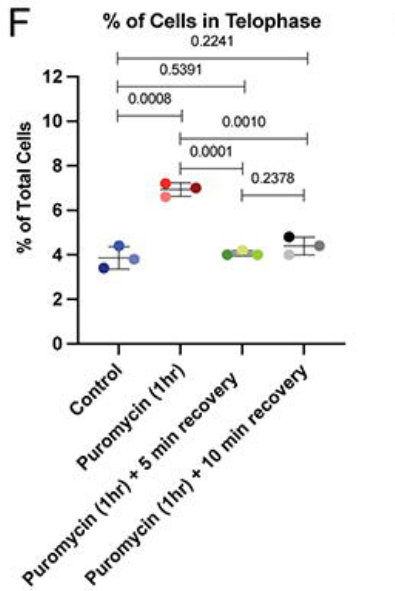
F
% of Cells in Telophase
% of Total Cells
12
10
8
6
4
2
0
0.2241
0.5391
0.0008
0.0010
0.0001
0.2378
Control
Puromycin (1hr)
Puromycin (1hr) + 5 min recovery
Puromycin (1hr) + 10 min recovery

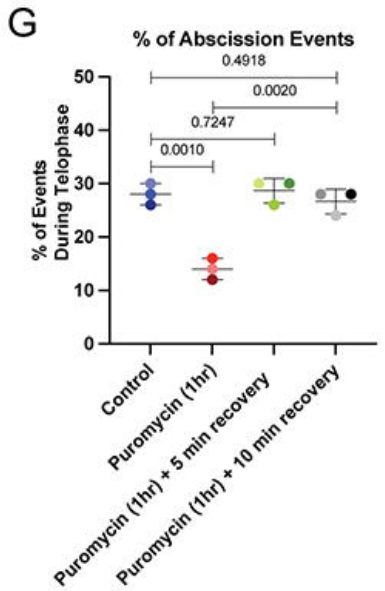
G
% of Abscission Events
% of Events
During Telophase
50
40
30
20
10
0
0.4918
0.0020
0.7247
0.0010
Control
Puromycin (1hr)
Puromycin (1hr) + 5 min recovery
Puromycin (1hr) + 10 min recovery

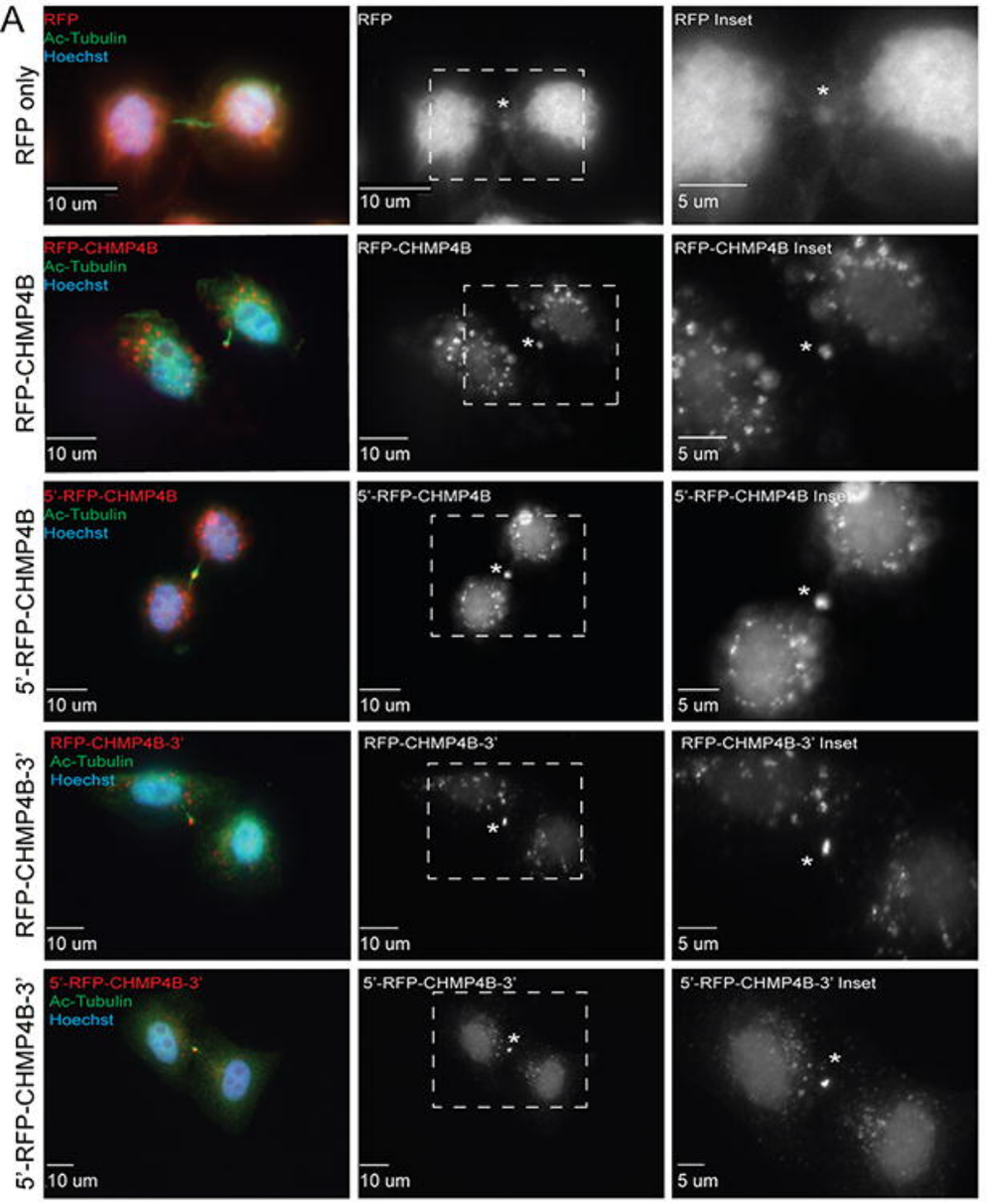
A
RFP only
RFP-CHMP4B
5'-RFP-CHMP4B
RFP-CHMP4B-3'
5'-RFP-CHMP4B-3'
RFP
Ac-Tubulin
Hoechst
RFP Inset
RFP-CHMP4B
RFP-CHMP4B Inset
5'-RFP-CHMP4B
5'-RFP-CHMP4B Inset
RFP-CHMP4B-3'
RFP-CHMP4B-3' Inset
5'-RFP-CHMP4B-3'
5'-RFP-CHMP4B-3' Inset
10 um
5 um

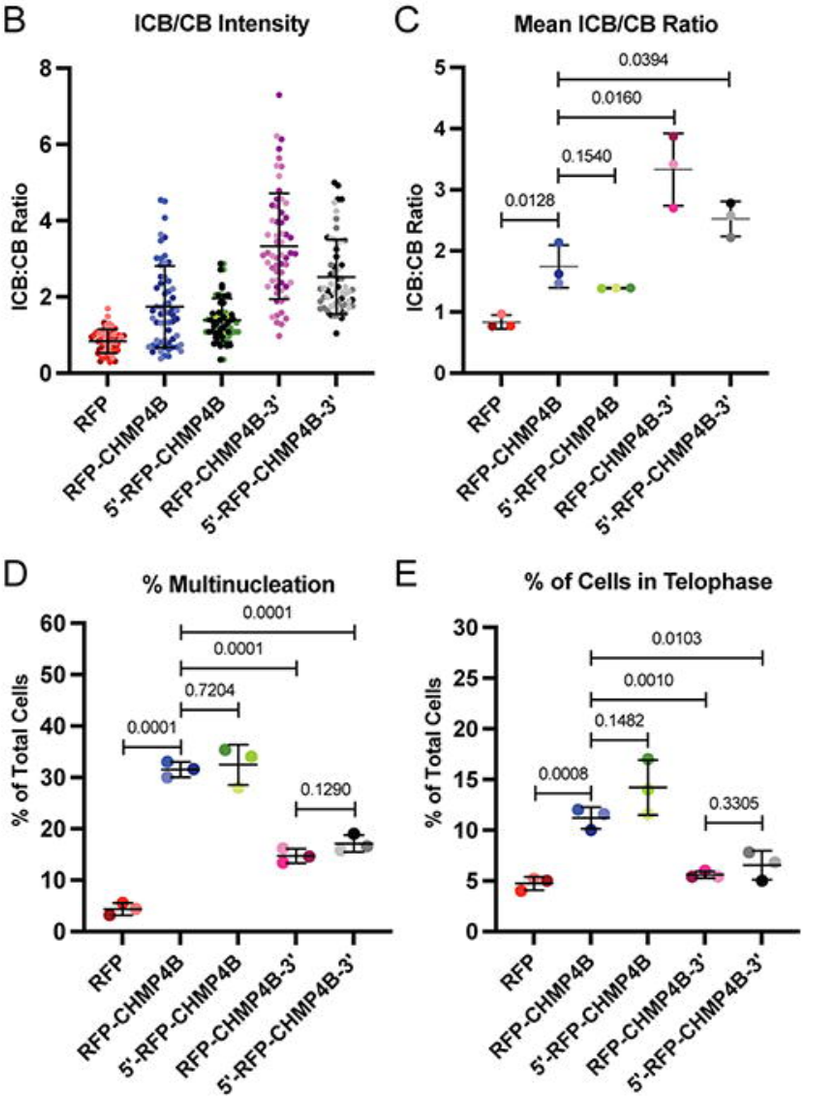
B
ICB/CB Intensity
ICB:CB Ratio
C
Mean ICB/CB Ratio
0.0394
0.0160
0.1540
0.0128
D
% Multinucleation
% of Total Cells
0.0001
0.0001
0.7204
0.0001
0.1290
E
% of Cells in Telophase
0.0103
0.0010
0.1482
0.0008
0.3305
RFP
RFP-CHMP4B
5'-RFP-CHMP4B
RFP-CHMP4B-3'
5'-RFP-CHMP4B-3'

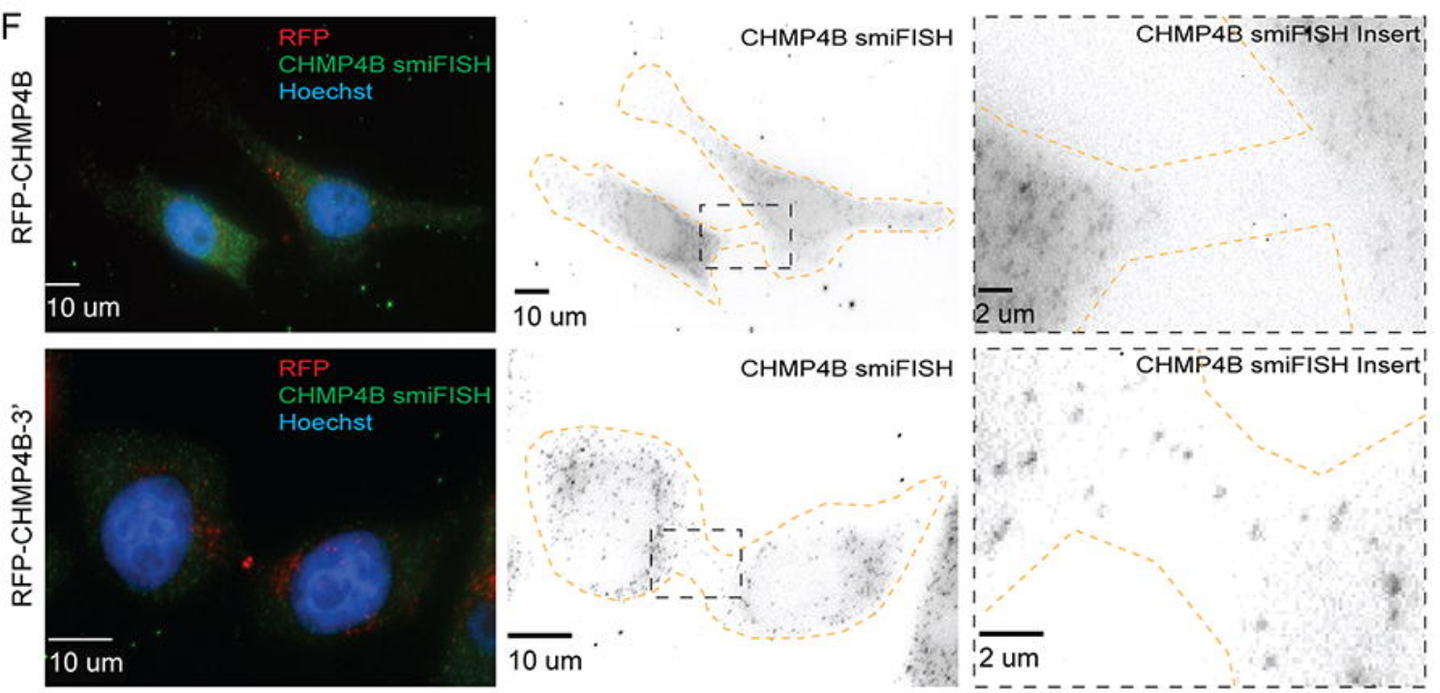
F
RFP-CHMP4B
RFP-CHMP4B-3'
RFP
CHMP4B smiFISH
Hoechst
CHMP4B smiFISH
CHMP4B smiFISH Insert
10 um
2 um

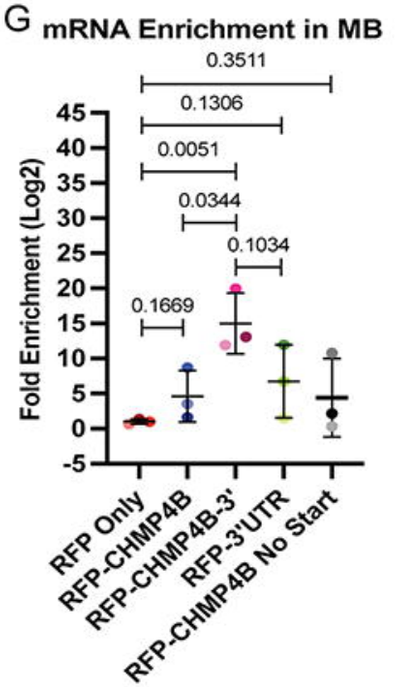
G
mRNA Enrichment in MB
Fold Enrichment (Log2)
0.3511
0.1306
0.0051
0.0344
0.1034
0.1669
RFP Only
RFP-CHMP4B
RFP-CHMP4B-3'
RFP-3'UTR
RFP-CHMP4B No Start

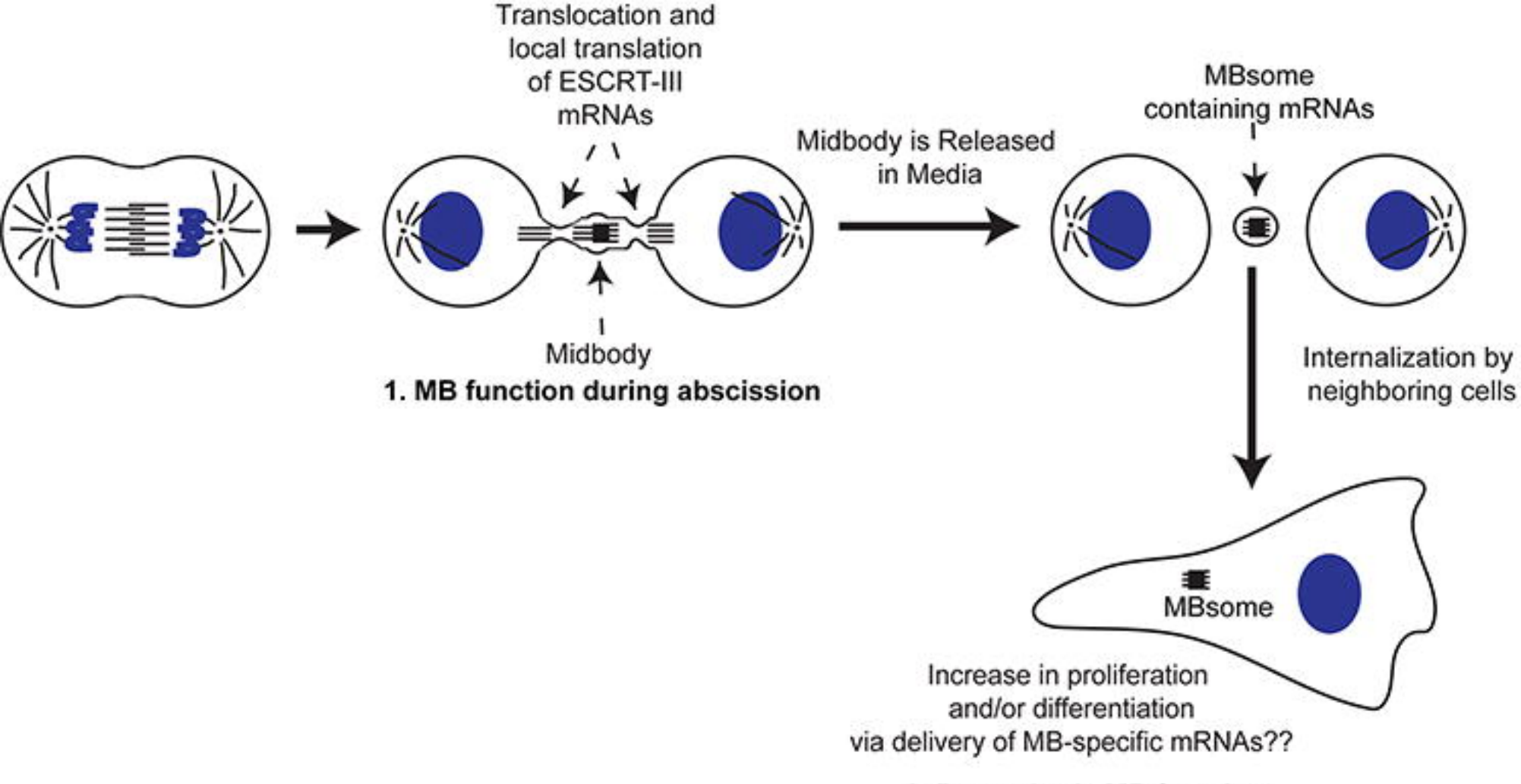
Translocation and
local translation
of ESCRT-III
mRNAs
Midbody
1. MB function during abscission
Midbody is Released
in Media
MBsome
containing mRNAs
Internalization by
neighboring cells
MBsome
Increase in proliferation
and/or differentiation
via delivery of MB-specific mRNAs??
2. Post-mitotic MB function